Excitation function for the math xmlns="http://www.w3.org/1998/Math/MathML">mrow>mmultiscripts>mi>Li/mi>mprescripts>/mprescripts>none>/none>mn>6/mn>/mmultiscripts>mo>+/mo>mi>α/mi>/mrow>/math> reaction between 0.5 and 1.4 MeV

A. Gula, R. J. deBoer, R. Kelmar, J. Görres, K. V. Manukyan, E. Stech, W. Tan, and M. Wiescher

Phys. Rev. C **106**, 065801 — Published 9 December 2022

DOI: 10.1103/PhysRevC.106.065801

Excitation Function for the ^{6}Li+α Reaction Between 0.5 and 1.4 MeV

A. Gula, R.J. deBoer, R. Kelmar, J. Görres, K.V. Manukyan, E. Stech, W. Tan, and M. Wiescher
Department of Physics and the Joint Institute for Nuclear Astrophysics, Notre Dame, Indiana 46556, USA
(Dated: November 28, 2022)

The recent discovery of Carbon Enhanced Metal Poor (CEMP) stars leaves open questions as to how carbon, nitrogen, and oxygen (CNO) elements were enriched through the nucleosynthesis of primordial elements in the first stars. It has been proposed that the reaction sequence ^{6}Li(α,γ)^{10}B(α,d)^{12}C may offer an alternative path to the traditional triple-α process, taking advantage of α cluster configurations in the ^{10}B and ^{14}N compound nuclei. In the present study, an investigation of the low-energy ^{6}Li$(\alpha,\gamma)^{10}$B cross section is performed using a combination of different γ ray detectors. The discrepancies in the literature of the width of the broad resonance ($E_{\rm c.m.}$ = 1200 keV, 1_3^+) are resolved. A consistent and much more precise width, Γ_α = 125(8) keV, is obtained via a simultaneous R-matrix fit of the data from the present study and that reported previously in the literature. The uncertainty in the tail contribution of the broad resonance indicates that a substantial increase in the low temperature reaction rate is possible compared to that adopted by the REACLIB compilation.

I. INTRODUCTION

Nucleosynthesis during the Big Bang occurs between the third and tenth minute [1]. The rapidly declining temperature and density conditions in the expanding environment prohibit the formation of a substantial amount of nuclei in and above the carbon range due to the mass 5 and 8 gaps. The resulting primordial baryonic abundances therefore consist primarily of ^{1}H and ^{4}He, with mass fractions $X_H \approx 0.5$ and $X_{He} \approx 0.5$. Heavier isotopes beyond the mass $A = 5$ gap, such a ^{6}Li and ^{7}Li - often produced in the form of ^{7}Be ($t_{1/2} \approx 53$ days) - are predicted to have been formed with the very small mass fractions of $\log_{10}$(^{6}Li/H) = -13.89±0.20 and $\log_{10}$(^{7}Li/H) ≈ -9.32±0.06, respectively [1].

The first stars emerged about 400 million years after the Big Bang via gravitational contraction of higher density inhomogeneities in the baryon distribution of its debris [2]. This material was characterized by a pure primordial abundance and provided the seed material at the onset of stellar nucleosynthesis. These stars are thought to have been very massive, typically between 15 and 150 $M_\odot$. In later stellar generations, such massive stars are stabilized by the CNO cycles [3] during the hydrogen burning phase. However, due to the scant abundances of CNO elements in the initial primordial fuel material, energy generation in first stars is based primarily on the *pp*-chains, expanding to include the hot *pp*-chains [4] in the gradually contracting cores. Simulations indicate [5] that the these types of stars continue to contract until sufficient temperatures and densities are reached for the triple-α process to generate enough ^{12}C to initiate the CNO cycle, thus re-establishing hydrostatic equilibrium. While this reaction comes to full fruition above 0.3 GK, alternative α induced reaction sequences may operate at considerably lower temperatures, between ≈0.05 and 0.3 GK, and may accelerate the production of CNO isotopes.

Indeed, the initial ^{6}Li abundance in primordial material, which was primarily formed by the ^{4}He$(d,\gamma)^6$Li reaction, opens another possible reaction branch towards the CNO range. The ^{6}Li$(\alpha,\gamma)^{10}$B$(\alpha,d)^{12}$C reaction sequence, which feeds deuterium back as fuel material, establishes a weak cyclic reaction sequence by which heavier elements are produced [6]. The efficiency of this process depends on the strength of the associated reaction rates as well as those of the competing ^{6}Li$(p,\alpha)^3$He [7, 8] and ^{10}B$(p,\alpha)^7$Be [9] reactions.

The reaction rate of ^{6}Li$(\alpha,\gamma)^{10}$B as well as the three subsequent reaction branches, ^{10}B$(\alpha,d)^{12}$C, ^{10}B$(\alpha,p)^{13}$C, and ^{10}B$(\alpha,n)^{13}$N, are expected to be characterized by pronounced α-cluster resonances near their thresholds [10]. This might cause a substantial increase in the reaction rate [6] of ^{6}Li$(\alpha,\gamma)^{10}$B compared to previous assessments [11], which have not taken into account possible broad resonances or direct capture contributions. This increase, in combination with an increase of helium rich bubbles in the highly convective early star environment [12], may generate a substantial reaction flow via this proposed branch, which may in turn lead to a faster production of CNO material in the first star environment.

In this work, we will discuss recent measurements of the ^{6}Li$(\alpha,\gamma)^{10}$B reaction while measurements of the subsequent ^{10}B+α reaction channels will be presented separately in other publications. Sec. II first discusses the different underlying components of the ^{6}Li$(\alpha,\gamma)^{10}$B reaction rate. Sec. III describes the experimental set-up for the measurements, followed in Secs. IV and VI by the analysis of the data and its interpretation in the framework of multi-channel R-matrix theory, respectively. A reaction rate is then calculated in Sec. VII based on the R-matrix calculations and narrow resonance strengths. Some conclusions, in terms of the impact on the reaction path, will be drawn in Sec. VIII.

II. REACTION COMPONENTS IN ^{6}LI$(\alpha,\gamma)^{10}$B

Because of the low level density in ^{10}B and the low Q-value of 4.461 MeV, the ^{6}Li$(\alpha,\gamma)^{10}$B reaction is characterized by only a few low energy resonances. The level structure in the ^{10}B compound nucleus is shown in Fig. 1. It displays a state at $E_x = 4.773$ MeV ($J^\pi = 3^+$), corresponding to a narrow, low energy, $\ell = 2$, resonance near $E_\alpha = 520$ keV. An earlier study observed a lower energy for this resonance, $E_\alpha = 500(25)$ keV [13], which has been used in the reaction rate calculations of Cyburt *et al.* [14]. The strength has been measured with an uncertainty of ≈10%, but upper and lower values differ significantly [15–17], indicating that systematic uncertainties hamper the results of earlier studies. Both of these factors lead to a great deal of uncertainty in the reaction rate. This resonance is the dominant component of the ^{6}Li$(\alpha,\gamma)^{10}$B reaction rate at the temperature range in an early primordial stellar environment ($0.05 < T < 0.3$ GK).

Three low-spin excited states between $E_x = 5.109$ and 5.170 MeV, in the compound nucleus ^{10}B, form a resonance group at $E_\alpha = 1.078$, 1.168, and ≈1.2 MeV. The two narrow resonances ($\Gamma \leq 1$ keV) at $E_\alpha = 1.078$ (2^-, $\ell = 1$) and 1.168 MeV (2^+, $\ell = 2$) have been measured several times, although there are still fairly large uncertainties associated with their resonance strengths [17–21].

The third resonance in the group at $E_\alpha \approx 1.2$ MeV corresponds to a $J^\pi = 1^+$ excited state in ^{10}B at a proposed excitation energy of 5.182 MeV. This level is rather broad; previous works have suggested total widths of $\Gamma = 200(30)$ [22], 105 [23], 110(10) [24] and 100(10) keV [25]. However, in Dearnaley *et al.* [23] it was explained that the 200 keV width reported by Sprenkel *et al.* [22] used an inaccurate formalism for the width calculation. They showed, using a simultaneous fit to their α-scattering on ^{6}Li data and Sprenkel *et al.* [22]'s ^{6}Li$(\alpha,\gamma)^{10}$B data, that the width should be considerably smaller, ≈105 keV. Similar widths were also observed by Armitage and Meads [24] and Auwärter and Meyer [25] using spectra from ^{10}B$(d,d)^{10}$B and ^{9}Be$(p,\gamma)^{10}$B measurements, respectively. Unfortunately, even the most recent rate compilation that includes the ^{6}Li$(\alpha,\gamma)^{10}$B reaction of Caughlan and Fowler [26] (CF88) has used the erroneously large width of Sprenkel *et al.* [22]. The tail of this broad resonance characterizes the cross section below 500 keV. The uncertainty in the tail contribution of this resonance, therefore, translates into a considerable uncertainty in the reaction rate at temperatures below 0.1 GK.

Even the revised width of ≈100 keV for the 1.2 MeV resonance translates into a reduced width of ≈1.8 MeV [23], twice the Wigner limit of ≈0.9 MeV, implying a unique nuclear structure. The spin and parity assignment of this level identifies the ^{6}Li+α entrance channel as $\ell = 0$ s-wave. It has been suggested that this level's very large reduced width can be interpreted as a pure α-cluster state, but for two identical α-particles [23, 27].

Finally, the direct capture (DC) component of the ^{6}Li$(\alpha,\gamma)^{10}$B reaction is not known. The direct capture is expected to be dominated by $E2$ transitions to the 3^+ ground state, the 1^+ first excited state at $E_x = 0.718$ MeV, and the 0^+ second excited state at $E_x = 1.740$ MeV in ^{10}B. Direct capture calculations, using the single particle potential model code `JEZEBEL` [28], have been performed to compare the strength of the direct capture contributions with the strength of the low energy tails of the 0^+ s-wave resonance at $E_\alpha \approx 1.2$ MeV. The simulation assumed a pronounced α-cluster structure for the bound states in ^{10}B [29, 30]. For example, [29] gives a spectroscopic factor of 0.6 for the 1^+_1 state. The cross sections of these DC components are well below that of the tail of the ≈1.2 MeV resonance at most energies. However, below $E_{\mathrm{c.m.}} \approx 0.17$ MeV, the calculations indicate that the ground-state DC component could become larger than the tale of the broad resonance, as discussed later in Sec. VII.

The experimental goal of this work is to accurately determine the width of the $E_\alpha \approx 1.2$ MeV cluster state, and provide a high statistics measurement of the strengths of the narrow resonances at $E_\alpha = 0.520$, 1.078 and 1.168 MeV. The high precision measurement of the resonances located in the low energy excitation function is necessary in order to better understand the limits and contributions of the broad resonance and the DC to the low temperature reaction rate.

III. EXPERIMENTAL METHODS

The 5U Pelletron accelerator at the University of Notre Dame [31] was used to measure the ^{6}Li$(\alpha,\gamma)^{10}$B reaction between E_α = 460-1400 keV. Beam intensities ranged between 1 μA and 15 μA because higher intensities resulted in rapid deterioration of the lithium targets. The most important feature of the Pelletron is its good energy resolution, ability to change energies rapidly and in arbitrary steps, and its stability over a wide range of energies. The beam energy of this machine was calibrated using the well-known resonances in the ^{27}Al$(p,\gamma)^{28}$Si reaction [32].

The target was mounted at 45° with respect to the beam direction and together with the target chamber formed the Faraday cup for measuring the beam current. A cold trap was used in order to prevent carbon buildup on the target surface. The trap consisted of a long LN_2 cooled copper pipe, which extended to within ≈ 3 cm of the target. The pipe was electrically isolated and biased at -300 V to suppress secondary electrons.

Evaporated lithium fluoride (LiF) targets have been shown to be unstable under high intensity α-particle beam bombardment [20, 33, 34]. Therefore, before yields were acquired from the ^{6}Li$(\alpha,\gamma)^{10}$B reaction, a LiF target study was performed. In these tests, it was found that the implementation of beam wobbling and water cooling prevented appreciable target deterioration under a certain threshold of integrated charge. A beam wobbler

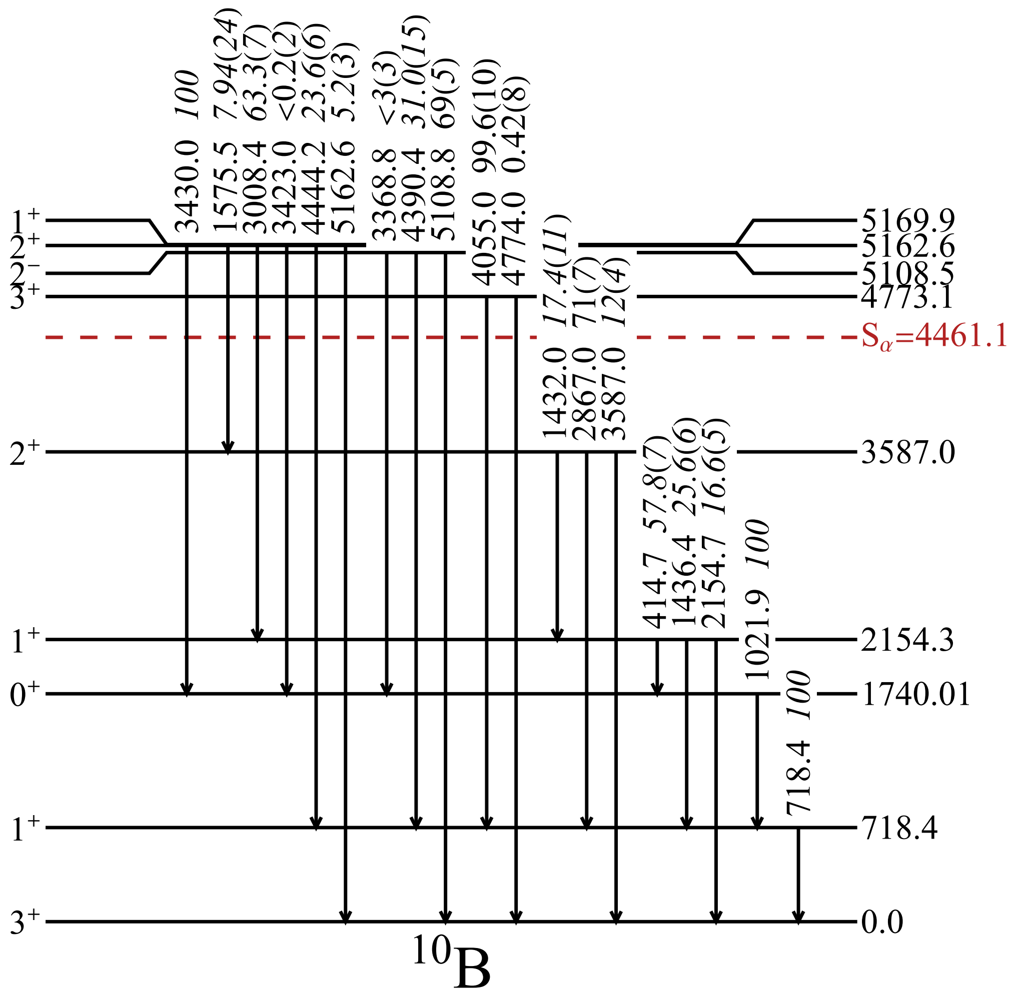

FIG. 1: Level scheme of the ^{10}B compound nucleus with γ ray transition energies and intensities shown from the present measurement. All energy values are given in keV. The present measurements are in general agreement with literature [17]. The α-particle separation (S_α) energy is indicated by the red dashed line.

enabled the focused beam spot on target to be uniformly dispersed over an area of about 4 cm^2.

From these tests, it was found that a ^{6}LiF target experienced a 15-25% degradation after an accumulation of 75 mC of integrated charge on target and that the target profile began to show significant signs of diffusion and surface enrichment of ^{6}Li nuclei. This could indicate that the ^{6}LiF had dissociated and the lithium had drifted away from the target backing while the fluorine may have drifted towards the target backing. Additionally, it was discovered that the threshold for these target stoichiometry effects to become significant was $\approx$60 mC. After $\approx$60 mC depositions, the high energy tail of the target integrated resonance scans demonstrated diffusion effects as well as a $\approx$15-20% drop in maximum yield on the plateau. In even smaller depositions, $\approx$50 mC, the deterioration that occurred was $\approx$5-10% and some faint surface enrichment was observed. Because of this, all of the targets in the current study were typically kept below $\approx$50-55 mC of charge deposited. Some gains in stability were seen with thicker targets, however it is also likely that the effect of drifting target nuclei in a thicker target is more easily obscured compared to a thin one.

Using ^{6}LiF enriched to $\geq$95%, targets of thicknesses

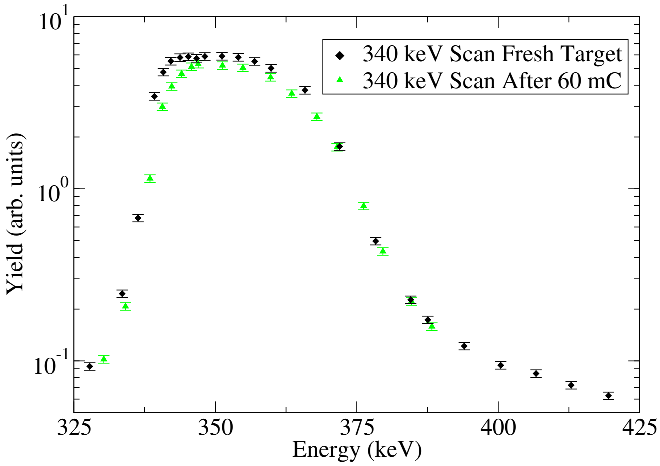

FIG. 2: ^{6}LiF target scan of the 340.5 keV resonance in the ^{19}F$(p, \alpha\gamma)^{16}$O reaction before and after bombardment. A scan of a fresh target is indicated by the black diamonds while that of a target exposed to 60 mC charge deposition by green triangles.

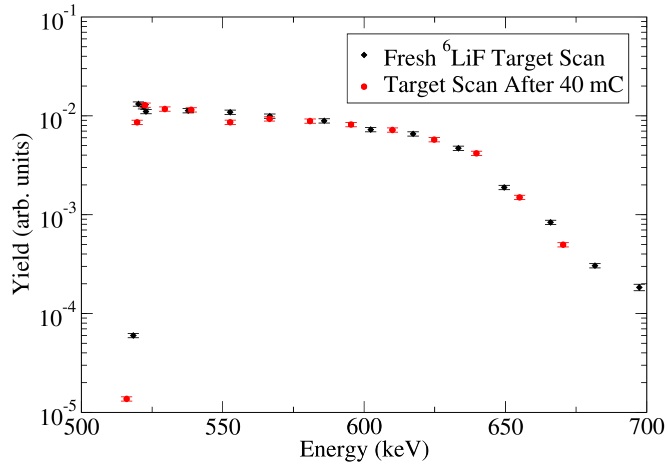

FIG. 3: ^{6}LiF target scan of the 520 keV resonance in the ^{6}Li$(\alpha, \gamma)^{10}$B before (black points) and after bombardment (red points).

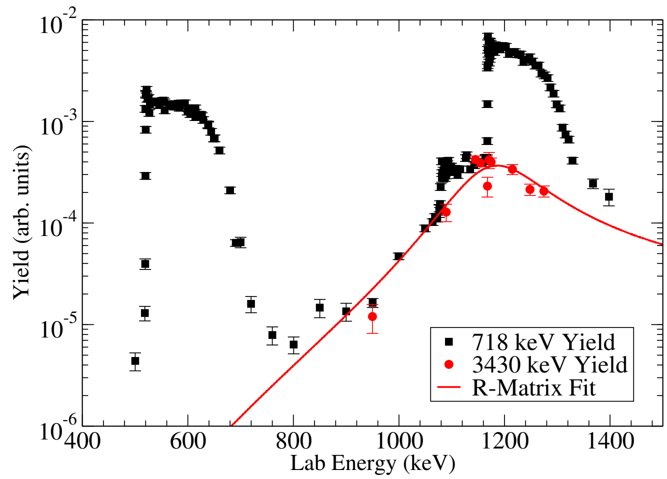

FIG. 4: Excitation function of the $E_\gamma = 718$ and 3430 keV-γ rays from the ^{6}Li$(\alpha, \gamma)^{10}$B reaction. The contribution from the underlying broad (Γ_α >100 keV) resonance can be observed separately through the yield of ≈3430 keV-γ rays and is shown by the red points. The solid red line indicates an R-matrix fit of this broad resonance (see Sec. VI).

between ≈10 μg/cm^2 and ≈50 μg/cm^2 were evaporated onto 0.5 mm tantalum backings. Targets were mounted 45° relative to the beam, making their effective thicknesses ≈14 μg/cm^2 and ≈71 μg/cm^2, respectively. This tantalum target backing served as the beam stop. Helium beam was impinged on a blank tantalum backing for ≈ 200 mC to determine what target backing contamination and background reactions might occur. In the present study, it was found that the ^{19}F$(\alpha, p\gamma)^{22}$Ne reaction was a substantial background above $E_\alpha = 1.4$ MeV. The γ ray produced at $E_\gamma = 1.274$ MeV did not greatly effect the $E_\gamma = 718$ keV region of interest, however the rate of detection for the emitted 1.274-MeV γ ray was high, $\geq$ 5000 cts/s. In addition to this fluorine induced background, a high intensity gamma line of 136 keV from ^{181}Ta$(\alpha, \alpha\gamma)^{181}$Ta inelastic scattering could be seen throughout the experiment.

Scans of the well known $E_p = 340.5$ keV resonance in the ^{19}F$(p, \alpha\gamma)^{16}$O reaction were used for target stoichiometry tests as well as for calibration of the detector and accelerator [35–37]. An example of the deterioration of these ^{6}LiF targets under 60 mC of bombardment is shown in Fig. 2. It is clearly seen that some ^{6}LiF is lost from the target, which amounts to ≈ 15% of the integrated yield. However, appreciable energy shifts ($\geq$ 1 keV) in target profile are not observed, though evidence for ^{19}F drift toward the target backing is observed. Scans of the $E_\alpha = 520$ keV resonance in the ^{6}Li$(\alpha, \gamma)^{10}$B reaction are also shown for comparison in Fig. 3.

A. Excitation Function Experiment

A CeBr$_3$ detector was placed at an angle of $\theta_{\text{lab}} = 55°$ at a distance of 2.5 cm from the target position to maximize efficiency and to minimize the contribution of the P$_2(\theta)$ Legendre polynomial in the angular distribution of the emitted γ rays. Due to the very close geometry of this detector, coincidence summing corrections need to be applied and are discussed in Sec. IV. The 2×2 in. CeBr$_3$ detector was a type 51B51/2M-CEBR(LB)-E2-X-NEG from Berkeley Nucleonics [38], and is referred to as “CeBr” through the remainder of the text. The measured excitation function is shown in Fig. 4. A diagram showing the experimental setup using this detector is given in Fig. 5.

In the excitation function, the $E_\alpha = 520$, 1078, 1168, and 1170 keV resonances are observed. Because of spin

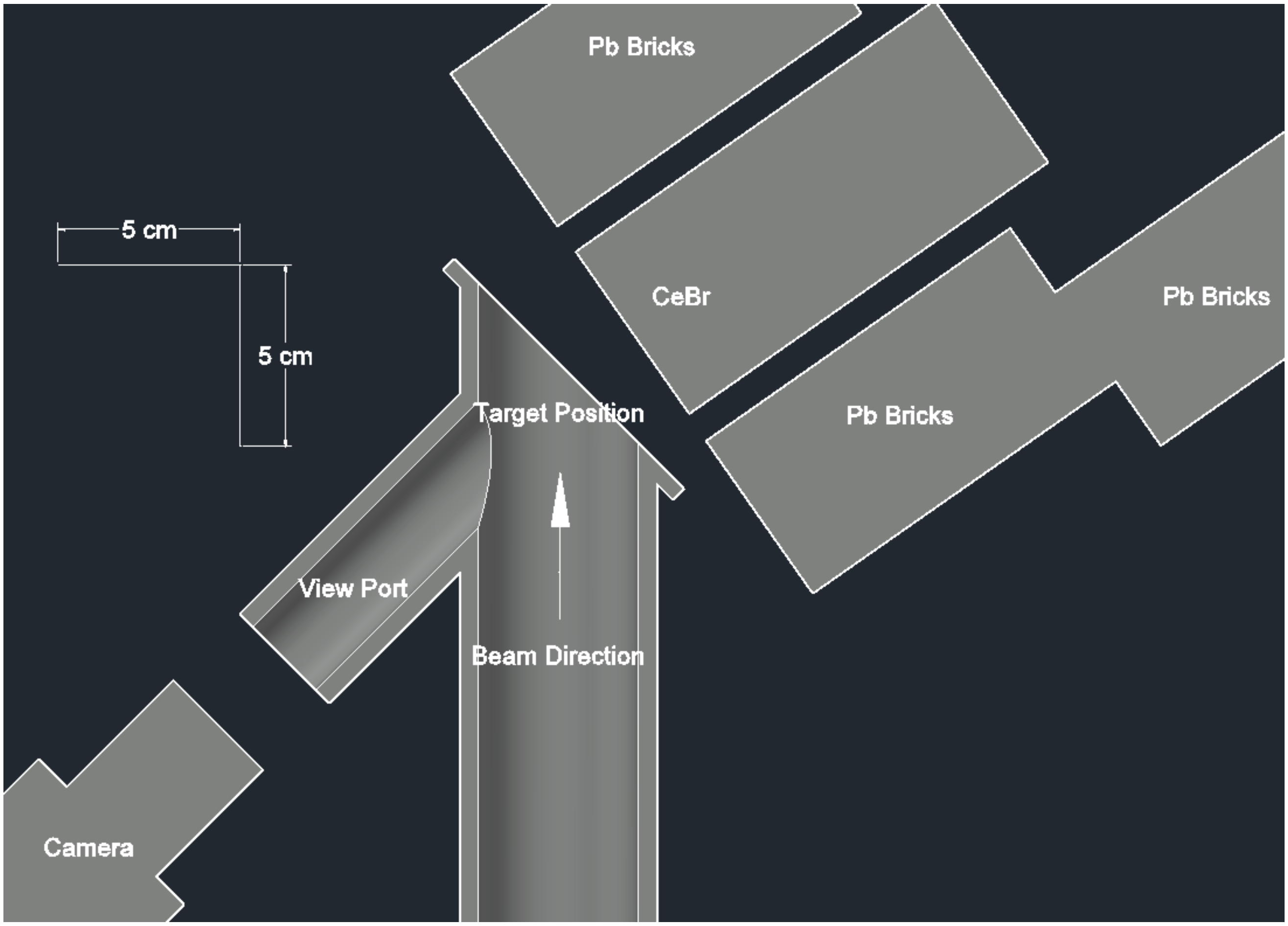

FIG. 5: Experimental setup diagram. The target was placed at 45° with respect to the beam direction. The CeBr detector was placed ≈2.5 cm from the target position at 55° relative to the beam direction. A camera was used to view the beam induced fluorescence from the ^{6}LiF targets, which assured a consistent bombarding location. A lead castle was assembled surrounding the detector crystal and electronics. The gaps seen between the lead bricks and the CeBr detectors is due to a low profile acrylic detector holder.

and parity selection rules, most transitions in the compound states of ^{10}B will decay through the 718 keV first excited state. Because of this, yield for the 718-keV γ ray, shown as black squares in Fig. 4, gives an excellent measure of the states populated in the $^{6}\mathrm{Li}(\alpha,\gamma)^{10}\mathrm{B}$ reaction. Since the intermediate transitions shown in Fig. 1 are weak compared to the 718-keV transition, these γ-ray yields are usually difficult to observe. This is especially true in the regions between resonances. However, the $E_\gamma = 3400$ keV yields from the broad resonance at $E_\alpha \approx 1.2$ MeV and branching ratios for these bound states were redetermined in the second experiment (Sec. III B) discussed later, which used a higher resolution high purity germanium detector (HPGe).

Energy and efficiency calibrations for the CeBr detector were performed using calibrated radioactive sources. The low-energy region was calibrated using a ^{137}Cs source [39] as well as a ^{133}Ba source [40]. The quoted radioactivity for these sources at purchase was 0.1014 ± 5% μCi [41] and 1.0 ± 5% μCi, respectively. For the intermediate energy regions, between the ^{137}Cs and the γ-rays from the $^{19}\mathrm{F}(p,\alpha\gamma)^{16}\mathrm{O}$ [35] reaction, ^{60}Co and ^{56}Co sources were used. The ^{60}Co source was quoted to have an activity of 11.59 ± 1.9% μCi, whereas the ^{56}Co source was uncalibrated. The ^{56}Co source was normalized using the 1238.288(3)-keV γ ray in ^{56}Co that lies between the 1173.228(3) and 1332.492(4)-keV γ rays of ^{60}Co [42, 43]. The data points of this efficiency curve were fit with a fourth order polynomial that described the log(efficiency) versus log(energy) trend of the calibration sources [44]. A systematic uncertainty of 5% was estimated from the uncertainties quoted on the radioactive sources.

The choice to use the CeBr detector over a HPGe detector for the excitation function is due to the higher efficiency of the CeBr detector. Fig. 6 shows a comparison between the efficiency calibrations for two HPGe detectors labeled “ORTEC” and “Georgina” (20% and 100%, respectively) and the CeBr detector. The HPGe detectors’ efficiencies fall very rapidly with increasing γ-ray energy, while that of the CeBr does so, but much more slowly. This slow tailing is particularly important in the present study since a measurement of the ground state direct capture was attempted. In addition, the ratio of CeBr to the 20% HPGe efficiencies is nearly a factor of fifteen at the 718-keV γ ray line of interest. However, at low-energies the thin beryllium window of the 20% HPGe detector accounts for the rapid rise in the efficiency curve labeled "ORTEC" in Fig. 6. A relative efficiency measurement of this CeBr detector indicates that it is 50% relative to NaI(Tl), however, because the CeBr detector could be placed in much closer geometries, the overall efficiency was higher.

Room background added an additional unfortunate complication to acquiring yields for the 718-keV γ ray from the ^{6}Li$(\alpha,\gamma)^{10}$B reaction. Due to the radioactive decay of uranium and thorium, bismuth-212 and bismuth-214 are produced. When these nuclei decay, they produce γ rays at $E_\gamma = 727.2$ keV and $E_\gamma = 719.9$ keV, respectively. For an HPGe detector, the γ ray at $E_\gamma = 727.2$ keV poses little concern, but the γ ray at $E_\gamma = 719.9$ keV is troublesome. In particular for data in the off-resonant regions, the unresolved ≈718-keV γ ray of interest and the 719.9 keV background line could be easily mistaken. However, because of both the low efficiency of the HPGe detectors and the difficulty in observing off-resonant yields, the CeBr detector [38] was used for the ^{6}Li$(\alpha,\gamma)^{10}$B study but the background was studied rigorously beforehand so that it could be subtracted.

In the studies of the background, it was found that a lead castle was able to reduce the background in the region of interest by nearly an order of magnitude.In these background studies, about three days of background was measured to provide good statistical significance. Background spectra are shown in Figs. 7, 8, and 9. In addition, care was taken to remove and replace lead bricks that had an unusually high concentration of uranium or thorium.

B. Angular Distributions and Broad Resonance Experiment

For the angular distributions presented in Sec. IV, two 100% HPGe detectors labeled as "Georgina" in Fig. 6 were used. The high resolution of these detectors was necessary for this portion of the experiment in order to resolve several transitions in the ^{6}Li$(\alpha,\gamma)^{10}$B reaction that occur at or around the $E_\gamma = 1.46$ MeV ^{40}K background line. In addition, two of the high energy resonances at $E_\alpha = 1.078$ and 1.168 MeV are quoted as having [17] very large $B(E2)$ and $B(M2)$ values for these transitions to the $E_x = 1.740$ MeV state in ^{10}B, indicating that the branching ratios for these transitions may be too large. This may be caused by contaminant yields for these transitions from the underlying broad resonance at $E_\alpha \approx 1.2$ MeV not being properly subtracted out as discussed further in Sec. V.

The HPGe detectors were both n-type, coaxial, EGC 100-260-R models from Canberra [46] and are the Georgina detectors mentioned previously. The efficiency calibration was accomplished using ^{137}Cs, ^{133}Ba, ^{56}Co, ^{60}Co, ^{152}Eu sources, and the ^{27}Al$(p,\gamma)^{28}$Si reaction. Similar to the CeBr efficiency calibration, the data points of the efficiency curve were fit with a fourth order polynomial that described the log(efficiency) versus log(energy) trend of the calibration sources [44]. This fit also accepts a systematic uncertainty of 5% due to the uncertainties quoted on the radioactive sources.

The first HPGe detector was placed 10 cm from the target position on a movable platform with the pivot point directly below the target position. This allowed for angular distributions on top of the narrow resonances near $E_\alpha \approx 1$ MeV. The second detector was placed 10 cm from the target position and fixed at a backward angle of 135°. This second detector allowed for the monitoring of target deterioration during the angular distribution measurements via the rates observed during each run. Finally, because of the higher resolution provided, an 3400-keV γ ray yield for the broad resonance transition could be extracted. This broad resonance yield is shown in Fig. 4 as the red points.

No lead castle was implemented in this setup since the 719.9 keV background line from bismuth-214 was not a concern with the high resolution of the detector. Additionally, the rate never exceeded 1000 cts/s due to the larger distances from the target.

IV. DATA ANALYSIS

Since the 718-keV γ ray transition from the first excited state is the dominant decay in the ^{6}Li$(\alpha,\gamma)^{10}$B reaction, it was used to determine the branching ratio corrected resonance strengths. Additionally, because of the better efficiency afforded by the detectors used in the present study, the branching ratios for all states below $E_x = 5.2$ MeV were remeasured in the present study and smaller uncertainties than in the previous literature were found in many cases. These γ-ray energies and branching ratios are presented in Table I.

The branching ratio analysis for the bound states was performed primarily with the 100% HPGe detector setup because of the energy resolution needed to resolve several ≈ 1.4-MeV γ rays emitted as part of the γ-ray decay cascade. The summed plateau yields measured at 55° on each resonance between E_α = 1 - 1.2 MeV provided a clear spectrum, which could be used to extract these branching ratios. From these analyses, it was found that most or all of the R/DC→ 0^+_1 photopeak counts came from the underlying broad $E_\alpha \approx 1.2$ MeV resonance. This indicated that the branching ratios in the literature [17] need to be adjusted down as given in Table I. These suggested adjustments would help to place these transition strengths more firmly within the $B(E2)$ and $B(M2)$ limits.

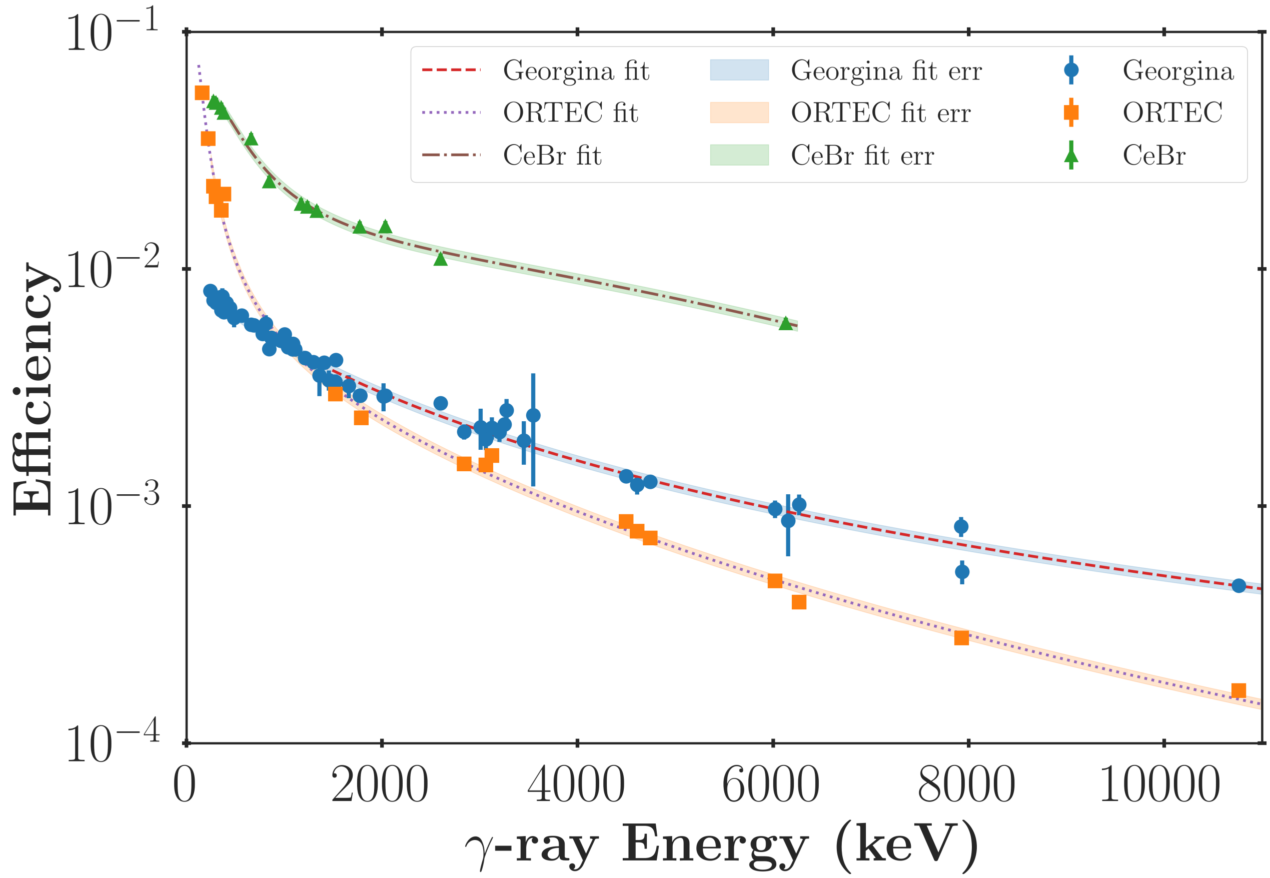

FIG. 6: Detector full energy peak efficiency comparison between the CeBr detector and two different HPGe detectors. Each detector calibration used sources and nuclear reactions to determine full energy peak efficiencies at various energies as describe in the text. The error band shown is a 5% band on this fit.

The angular distributions, shown in Fig. 10 were taken with the HPGe detector setup discussed in Sec. III B. Measurements at each angle had the same amount of charge deposited except at 0° and 135°, which were run slightly longer. The relative angular distribution data from Basak [47] for the $E_\alpha = 1.078$ and 1.168 MeV resonances were normalized to the 55° data point of the present measurements. This was done because the majority of measurements found in Basak [47] were taken at 52°. Overall, good agreement is observed between the measured angular distributions in the present study and those measured by Basak [47].

Spectra produced on top of each narrow resonance using the CeBr detector are shown in Figs. 11, 12, and 13, with each γ ray present in the spectrum identified and contamination sources attributed. Branching ratios for emissions from each level are given in Table I, where literature values are taken from the NNDC [17]. The branching ratios that were calculated from the HPGe detector and the CeBr detector are in excellent agreement. The values given in Table I and Fig. 1 are the weighted mean of these two measurement techniques.

The three narrow resonances in the excitation function of the ^{6}Li$(\alpha,\gamma)^{10}$B reaction between $E_\alpha = 0.46$-1.4 MeV were measured with a level of high statistics varying between over 5000 to over 25000 counts for the 718-keV γ ray on the plateau. Each narrow resonance was analyzed using the thick target yield technique, see Fig. 4.57 of [48]. This analysis was appropriate since the broadest of these narrow resonances was the one studied at $E_\alpha = 1078$ keV, which has a total width of ≈ 1 keV, while the beam energy loss through the targets ranged from 110 to 130 keV at $E_\alpha = 1.078$ MeV.

On each narrow resonance plateau, energy steps of 5 keV were taken until ≈15 keV before the front edge. Smaller steps, ≈1-2 keV, were then taken over the front edge. However, during resonance scans, to check for target deterioration, energy steps as large as 25 keV were taken in order to prevent excessive charge accumulation.

Due to the very close geometry of the detector to the target, coincidence summing corrections were performed following the two procedures laid out in McCallum and Coote [49] and Yoon *et al.* [50]. This was done to compare the intensities of sum peaks observed to the predicted

TABLE I: Branching ratios of states below E_x = 5.2 MeV in ^{10}B.

E_x (MeV)	E_α (MeV)	E_γ (keV)	Final state (MeV)	Branching ratio	Branching ratio (lit.) [17]
5.1699(25)	1.180(4)	3430.0(20)	1.740	100	100
5.1626(12)	1.1683(20)	5162.6(20)	0.0	5.2(3)	4.4(4)
		4444.2(20)	0.718	23.6(6)	22.6(6)
		3423.0(25)	1.740	<0.2(2)	≤0.5
		3008.4(20)	2.154	63.3(7)	65.3(9)
		1575.5(20)	3.587	7.94(24)	7.8(3)
5.1085(12)	1.0782(20)	5108.8(20)	0.0	69(5)	64(7)
		4390.4(20)	0.718	31.0(15)	31(7)
		3368.8(20)	1.740	<3(3)	5(5)
4.7731(3)	0.5196(5)	4774.0(20)	0.0	0.42(8)	0.5(1)
		4055.0(20)	0.718	99.6(10)	>99
3.5870(20)	–	3587.0(20)	0.0	12(4)	19(3)
		2867.0(20)	0.718	71(7)	67(3)
		1847.0(20)	1.740	<0.1(1)	≤0.3
		1432.0(20)	2.154	17.4(11)	14(2)
2.1543(20)	–	2154.7(20)	0.0	16.6(5)	21.1(16)
		1436.4(20)	0.718	25.6(6)	27.3(9)
		414.7(20)	0.718	57.8(7)	51.6(16)
1.7401(20)	–	1740.0(20)	0.0	0.0	≤0.2
		1021.9(20)	0.718	100	100
0.7184(20)	–	718.4(20)	0.0	100	100

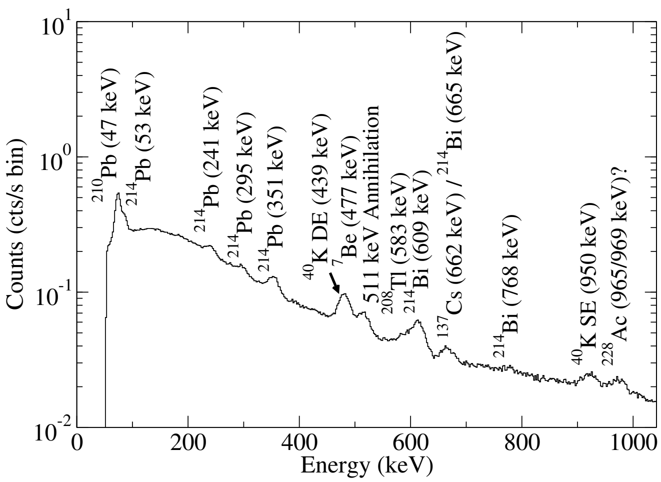

FIG. 7: Background spectra acquired with the CeBr detector at low energies. In the low energy region, the primary contaminants seen throughout the spectrum are ^{214}Bi and, the parent nucleus, ^{214}Pb with several weaker lines from uranium decay chain nuclei. The ^{214}Bi γ ray at 719.9 keV has been largely suppressed due to the lead shielding. For reference, the 609-keV γ ray is two orders of magnitude more intense and the 768-keV γ ray is one order of magnitude more intense than the 719.9-keV γ ray [45].

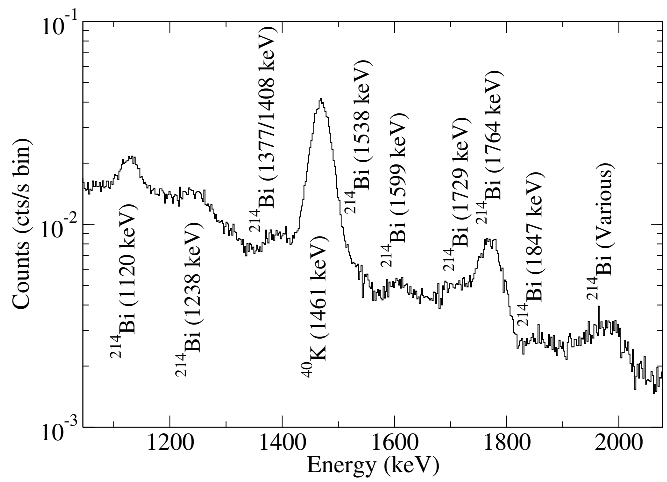

FIG. 8: Background spectra acquired with $\theta_{\text{lab}} = 55°$ CeBr detector at higher γ-ray energies. The ^{214}Bi γ rays continue to be observed throughout the spectrum with the addition of the strong ^{40}K γ ray.

sum peaks using the total efficiency acquired from the use of calibration sources. Because of the beam rastering, the source produced during bombardment would have been broader than the calibration sources used, thus the total efficiency could have varied. However, both methods were discovered to agree well with each other and the

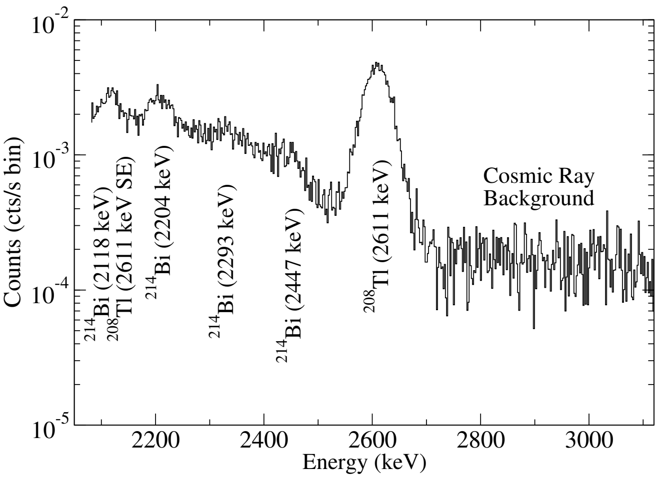

FIG. 9: Background spectra acquired with $\theta_{\mathrm{lab}} = 55°$ CeBr detector at the highest γ-ray energies. The ^{214}Bi γ rays and the strong ^{208}Tl γ ray are the only remaining radiogenic lines present in the high energy spectrum. Though not shown here, the cosmic ray background smoothly decays out to the end of the ADC spectrum at over 12 MeV.

corrections to the $E_\gamma = 718$ keV yield were performed. The corrections resulted in an increased yield. For the $E_\alpha = 1168$ keV resonance the correction was $\approx 15\%$, whereas for the $E_\alpha \approx 520$ keV resonance was only $\approx 4\%$. This correction is very similar to that reported by Gyürky *et al.* [11], who estimated a correction of $\approx 10\%$ for the $E_\alpha = 1168$ keV resonance.

As mentioned in Sec. III, an energy calibration of the accelerator was performed using the well-known ^{27}Al$(p,\gamma)^{28}$Si reaction. This energy calibration produced <1 keV deviation from the narrow resonances in the ^{27}Al$(p,\gamma)^{28}$Si reaction and the energy resolution at the front edge of the $E_p = 992$ keV resonance was <100 eV. Sec. V discusses how several of the narrow resonances studied here were found to sometimes be at significantly different energies than those quoted in the literature [18, 19, 47].

During the present experiment, several sources of systemic uncertainties were identified and are presented in Table. II. The most dominant systematic uncertainties are from the stopping power calculation [53] and the efficiency calibration of the detectors. Included in the efficiency uncertainty is the geometric variances of the detector position and angle as well as the calibration uncertainties. Additional uncertainties in charge collection are suspected, either from the incomplete collection of secondary electrons from the target or due to beam instabilities. Finally, the stoichiometry of the target LiF material was stable during initial thick target scans, however small uncertainties are associated with this determination of the active density.

TABLE II: Summary of systematic uncertainty estimates.

Systematic Uncertainty Contribution	%
Charge Collection	3
Stopping Power	5
Efficiency	5
Stoichiometry	1
Thick Target Analysis Techniques	1
Total	7.8

V. DISCUSSION

A. The 4.773 MeV Level

The $J^\pi = 3_2^+$ narrow resonance located at $E_{\mathrm{lab}} = 521.1(8)$ keV in the literature [17] is currently found to be at $E_{\mathrm{lab}} = 519.6(5)$ keV. While these values are consistent at about the 1.5σ level, this difference in energy is quite significant as the low temperature reaction rate depends exponentially on the resonance energy, as shown later in the discussion of the reaction rates in Sec. VII. This is the lowest energy resonance known to exist in the ^{6}Li$(\alpha,\gamma)^{10}$B reaction. Very few measurements have been made of it, though they do find moderate agreement in the resonance strength. Early charged particle and transfer reaction measurements had observed the corresponding state in ^{10}B [54], but the first ^{6}Li$(\alpha,\gamma)^{10}$B measurement was performed in 1953 by Wilkinson and Jones [13], where an energy of $E_\alpha = 500(25)$ keV was reported. The strength of this resonance remained unknown until Warhanek [51] measured it to be $\omega\gamma \approx 5\times10^{-2}$ eV in 1957. Shortly thereafter, Alburger *et al.* [16] (1966), found a very similar value of $\omega\gamma = 0.046(8)$ eV.

In later studies performed by Nelson *et al.* [15] in 1985, a much smaller resonance strength was observed. In particular, the thick target yields presented in Nelson *et al.* [15] indicated $\omega\gamma = 0.041(4)$ eV from a relative measurement of the 520 keV resonance with respect to that at $E_\alpha = 1168$ keV. Though the Alburger *et al.* [16] and Nelson *et al.* [15] resonance strengths agree, the yield curves presented in Fig. 1 of Nelson *et al.* [15] seem to indicate resonance energies closer to $E_\alpha \approx 520$ and $\approx$1168 keV, but their calculations used 500 and 1175 keV, respectively. This energy difference changes the relative resonance strength calculation, causing the strength to go from $\omega\gamma = 0.041(4)$ eV to $\omega\gamma = 0.0425(43)$ eV when the present resonance energies are used. The 718 keV state feeding coefficients (f) – where f is given by the sum of all branching ratio products corresponding to the cascades terminating in the observed transition – found in the present study are $f(4.773) = 0.996$ and $f(5.163) = 0.828$. Using these f instead of those found in [15], then $\omega\gamma_{Nelson} = 0.0440(44)$ eV, which is

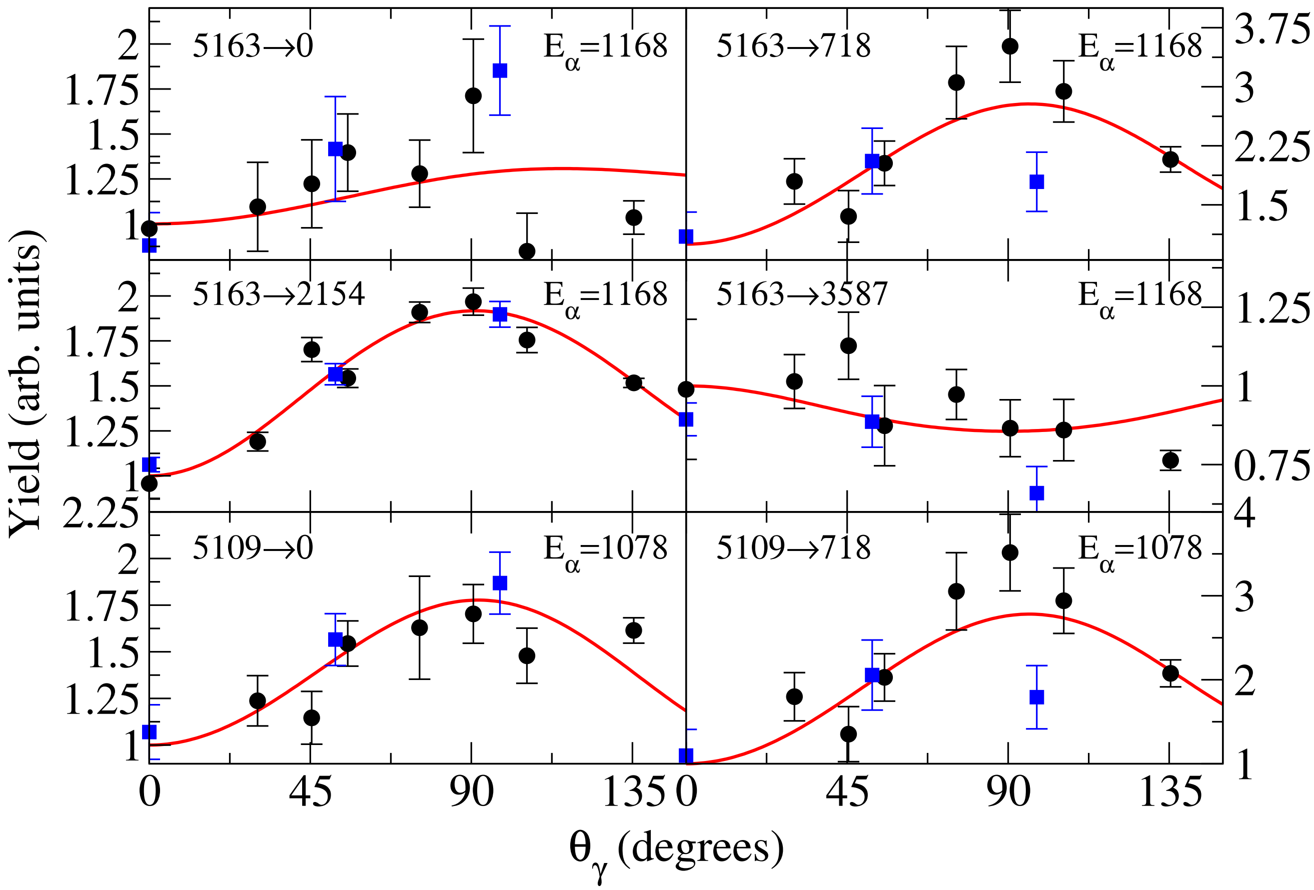

FIG. 10: Angular distributions for primary γ-ray transitions from the resonances at $E_{\mathrm{c.m.}} = 1078$ and 1168 keV in the ^{6}Li$(\alpha,\gamma)^{10}$B reaction. The angular distributions presented here, shown as black circles, were measured with the n-type HPGe detector. The data of Basak [47], shown as the blue squares, were normalized to the present data at 55°. The red line is the R-matrix angular distribution fit performed using AZURE2.

much closer to the value obtained by Alburger *et al.* [16] and the present study: $\omega\gamma = 0.046(8)$ eV and $\omega\gamma = 0.0472(37)$ eV, respectively.

The resonance strength presented in the TUNL compilation [17] is reported as the weighted mean of the Nelson *et al.* [15] and Alburger *et al.* [16] data with $\omega\gamma = 0.0420(36)$ eV. However, the weighted average of the Nelson *et al.* [15] and Alburger *et al.* [16] $\omega\gamma$ is actually 0.0445(39) eV. Additionally, the value presented in NNDC appears to be just that of Nelson *et al.* [15]. As discussed above, these should be re-evaluated considering the corrected strength. In addition, the present study is in excellent agreement with the other resonance strengths discussed in the following subsections, which suggests a good degree of reliability in the $\omega\gamma = 0.0472(37)$ eV found in the present study. A table compiling these suggested $\omega\gamma$ revisions is given in Table III.

B. The 5.109 MeV Level

The J$^{\pi} = 2_1^-$ state at $E_x = 5.11(2)$ MeV, corresponding to a resonance energy of $E_{\mathrm{lab}} = 1.08(1)$ MeV, has been measured thoroughly by Napolitano and Freedman [18], Ajzenberg-Selove [55]. In the present study, good agreement is found with this value, where the resonance was observed at $E_{\mathrm{lab}} = 1.0782(20)$ MeV, corresponding to $E_x = 5.1085(12)$ MeV. This state has been measured previously [18, 19, 47, 52, 56], with differing experimental techniques. The most important difference in these previous studies is that of the resonance strength determination. One of the first of these measurements, in 1957 [52], found the strength of this resonance to be $\omega\gamma = 0.105(26)$ eV, where the uncertainty is roughly estimated as ≈25%.

The next experiment by Forsyth *et al.* [19], performed in 1966, found a smaller strength of $\omega\gamma = 0.092(17)$ eV. In addition, that study was able to measure the γ-decay branching ratios fairly accurately. These branching ratios and strength remain consistent with modern accepted values in literature today [57].

TABLE III: Revised Resonance Strengths. Literature values are taken from [17].

E_x(MeV)	E_α(MeV)	$E_{lit.}$(MeV)	$E_{\alpha-lit.}$(MeV)	$\omega\gamma_{(\alpha,\gamma)}$	$\omega\gamma_{(\alpha,\gamma)}$(lit.)	$\omega\gamma_{(\alpha,\gamma)}$(rev.)
5.1626(12)	1.1683(20)	5.1639(6)	1.1704(10)	0.389(30)	0.40(4)	–
5.1085(12)	1.0782(20)	5.1103(6)	1.0812(10)	0.0456(36)	0.055(10)	0.049(9)
4.7731(3)	0.5196(5)	4.7740(5)	0.5211(8)	0.0472(37)	0.0420(36)	0.445(35)

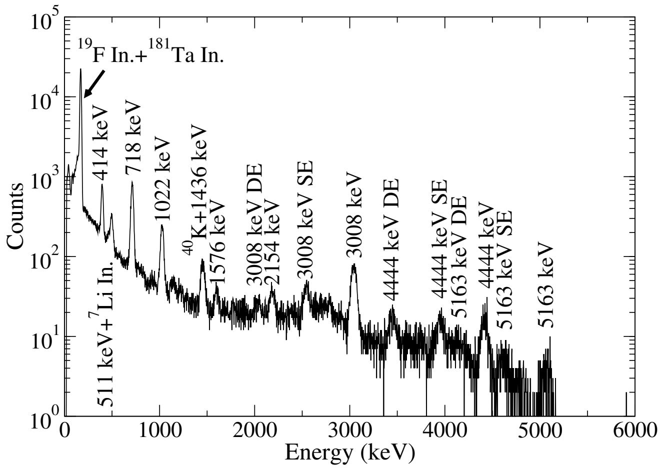

FIG. 11: Sample spectrum from the CeBr detector on the $E_\alpha = 1.168$ MeV resonance. The 1.168 MeV resonance scan contains the most complicated spectrum observed in the present ^{6}Li$(\alpha,\gamma)^{10}$B experiment. Several high energy γ rays from the 5162 keV state are visible. The GS transition is seen with a fairly strong intensity, however the 3008 and 4444 keV γ rays dominate the higher energy spectrum. These feed the lower energy states in ^{10}B, which mostly feed the 718-keV γ ray that is seen strongly in the spectrum. Beyond the γ rays from the reaction of interest, prominent background lines from ^{19}F, ^{181}Ta, and ^{7}Li inelastic scattering are present. In addition, the 511-keV γ ray and the room background ^{40}K line at 1.46 MeV are prominent.

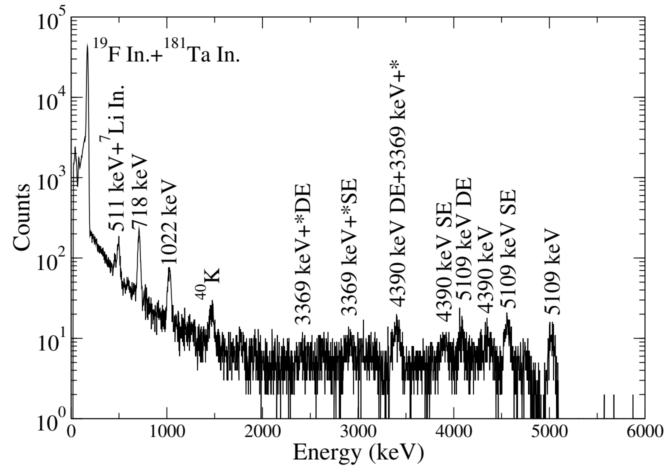

FIG. 12: Sample spectrum from the CeBr detector on the $E_\alpha = 1.078$ MeV resonance. In previous studies [19, 47], significant errors were made in the measurement of the 1.078 MeV resonance. This was due to several factors, including the overall small strength of the resonance as well as the $E_\alpha \approx 1.2$ MeV broad resonance contaminating the 718-keV γ ray feeding in the spectrum. The primary transition from the broad resonance and its escape peaks are shown with an asterisk in this figure.

A subsequent Napolitano and Freedman [18] study measured the Γ_α of this resonance to be 0.98(7) keV, which is still used in literature today. However, a calculation of the resonance strength was not performed. Additionally, the broad resonance at $E_\alpha \approx 1.2$ MeV corresponds to the $\approx$5.182 MeV $J^\pi = 1^+$ state in ^{10}B, was unobserved in this study. The 1966 study of Forsyth *et al.* [19] observed the contamination of this broad state to correspond to $\leq$15 % of the 1.078 MeV γ-ray intensity. However, in the present study, it was found to be $\approx$25% at the plateau. However, the branching ratios measured in the present study are still in fair agreement with Forsyth *et al.* [19].

One of the most recent studies by Basak [47] in 1989 found very different results for the 5.108 MeV state. The first disagreement is a drastic decrease in the resonance strength measurement, which was found to be $\omega\gamma = 0.046(4)$ eV. The second strong disagreement was in the branching ratios, where Basak [47] found $\beta_{5.109\rightarrow1.740} = 0.109(35)$, compared to $\beta_{5.109\rightarrow1.740} = 0.05(5)$ found in Forsyth *et al.* [19]. This large change in $\beta_{5.109\rightarrow1.740}$ was addressed in the ^{10}B TUNL data compilation in 2004 [17], where the branching ratios of Basak [47] were rejected due to the $B(M2)$ value being much larger than the Recommended Upper Limit (RUL) of the Weisskopf estimates for γ-ray transitions. The 1989 study of Basak [47] was one of the few to perform angular distribution measurements. However, many of these have few angles of measurement and have large uncertainties.

Finally, in the discussion of Spear *et al.* [20], many of the resonance strengths are given in the center of mass frame of reference but appear to have failed to correctly apply the center-of-mass conversion factor $\approx \frac{6}{10}$. This factor also appears to have been omitted in Forsyth *et al.* [19] and Meyer-Schutzmeister and Hanna [52]. When the center of mass conversion fac-

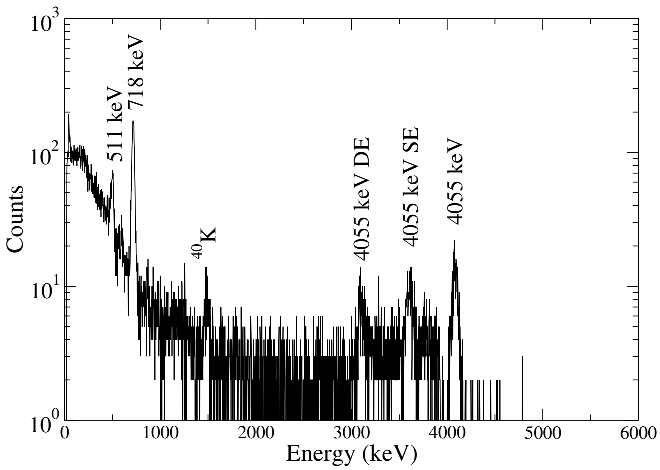

FIG. 13: Sample spectrum from the CeBr detector on the $E_\alpha = 0.520$ MeV resonance. In previous studies, the strength of the 0.520 MeV resonance was disputed and difficult to measure due to its low yield. In the present study, great effort was placed on studying this resonance and accurately determining its strength. In addition, the GS feeding found in prior literature [51, 52] appears to overestimate the branching ratios. However, the present study is in good agreement with the compilation [17]. This may be due to incomplete analysis of coincidence summing in the γ-ray detectors.

tor is applied to these measurements, they are still quite high with respect to the present study's finding of $\omega\gamma = 0.0456(36)$ eV. Though the average found in Table 10.22 of [17], $\omega\gamma = 0.055(10)$ eV, is in agreement within error bars with the present study, a great deal of uncertainty on the high values of this average exists; namely, the lack, or underestimation of, the broad resonance contributions to the yields.

As stated earlier, the Forsyth *et al.* [19] study estimated this contribution to be $\leq$15%, and Meyer-Schutzmeister and Hanna [52] and Napolitano and Freedman [18] do not discuss this contribution. In the present study, the broad resonance contributions were found to be about 25% of the total γ-ray yields around this resonance. If the Forsyth *et al.* [19] study is corrected to include this higher broad resonance contribution, then their original $\omega\gamma = 0.092(17)$ eV resonance strength would be reduced to 0.081(15) eV. Then, with the center of mass factor reapplied [20], a resonance strength of $\omega\gamma_{\text{Forsyth - c.m.}} = 0.049(9)$ eV is found. This value is much closer to the present studies finding of $\omega\gamma = 0.0456(36)$ eV and is also in agreement with [47], despite the problems mentioned with that study.

Finally, the angular distributions of $5.163 \rightarrow 2.154$, $5.109 \rightarrow 0.0$, and $5.109 \rightarrow 0.718$ transitions were remeasured and found to be in good agreement with those found in Basak [47]. Because of these considerations, it appears that the resonance strength for the 5.108 MeV state is near the 0.046(4) eV value found by Basak [47].

C. The 5.163 MeV Level

Very little deviation in the branching ratios, γ-ray energies, or resonance strengths are observed between the present study and the TUNL and NNDC compilations. However, there is a moderate difference in the resonance energies found in the present study compared to that reported in these compilations. Both compilations adopt $E_{J^\pi=2^+_2} = 5163.9(6)$ keV, whereas the present study finds this resonance appears to be located at $E_x = 5162.6(12)$ keV corresponding to $E_\alpha = 1.1683(20)$ MeV.

The largest energy deviation found in the present study comes from this $J^\pi = 2^+_2$ state. In literature, this resonance was cited to be observed near $E_\alpha = 1.175$ MeV in many prior studies [18, 19, 47], but the compilation value indicates an adopted value of $E_\alpha \approx 1.170$ MeV. However in the present study, this resonance is observed at $E_\alpha = 1.1683(20)$ MeV. It is unclear if the current compilation [17] has retained the high energy values from the prior studies [18, 19, 47] that cite $E_\alpha = 1.175$ MeV, however it is clear that the present study deviates from the literature value of $E_\alpha \approx 1.170$ MeV by $\approx$2 keV. This 2 keV energy shift does not have a substantial impact on the reaction rates discussed in Sec. VII, due to the high energy of this resonance. However, for stellar temperatures near 1 GK, this shift may have a small boosting effect.

D. The 5.170 MeV Level

In several previous studies, the underlying broad resonance located at $E_x = 5.1699(25)$ MeV was often ignored [18, 52, 56] or underestimated [19]. There has been some confusion about the total width of this level, but, as described in Sec. I, previous studies clearly indicate a value of $\Gamma_{\text{c.m.}} \approx$100 keV

In 1961, measurements of the ^{6}Li$(\alpha,\gamma)^{10}$B reaction were performed by Sprenkel *et al.* [22]. Two large NaI detectors were placed at 90° with respect to the beam and 3/4 in. away from the target. These detectors were used to perform coincidence measurements with the 718-1022-keV cascade γ rays in order to extract a yield for the $E_\alpha \approx 1.2$ MeV resonance. From this work, a reported $\Gamma_{\text{c.m.}} = 200(30)$ keV was measured and a reported $\Gamma_\gamma = 0.06(3)$ eV was given. However, only experimental yields for this resonance were presented (see Fig. 2 of [22]).

If, according to Sprenkel *et al.* [22], the $\Gamma_{\text{c.m.}}$ of 200 keV was true, then this would correspond to a very large dimensionless reduced width of $\theta^2 = \gamma^2/\gamma^2_{\text{W}} = 7.26$, well above even twice the Wigner limit ($2 \times \gamma^2_{\text{W}} = 1.8$ MeV, see Sec. II). Because of this apparent discrepancy, a measurement of ^{6}Li$(\alpha,\alpha)^6$Li was performed in 1962 by Dearnaley *et al.* [23]. In this α-scattering measurement, a very well resolved broad resonance was observed at four laboratory angles at $\approx$1.2 MeV with a calculated center of mass $\Gamma_{\text{c.m.}} \approx 105$ keV. Dearnaley *et al.* [23] performed a

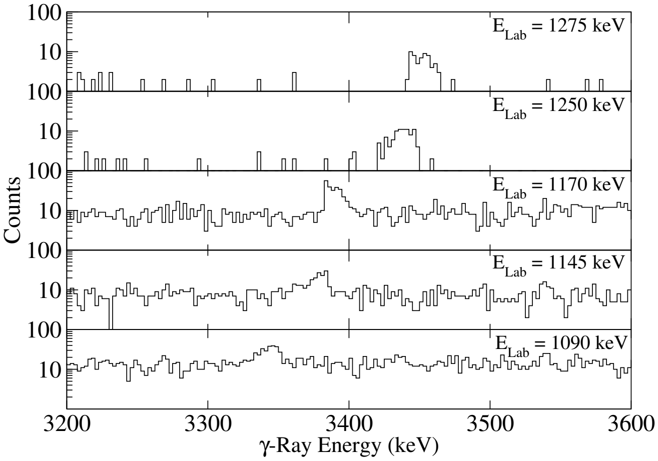

FIG. 14: Observed shift of the $1^+_3 \to 0^+_1$ transition at various energies. The broadened peak structure observed is due to the thickness of the target. A target of $\Delta E \approx 30$ keV was used for this portion of the study.

multichannel R-matrix fit and found that their data and those of Sprenkel *et al.* [22] were in fact consistent. They then showed that the formalism used by Sprenkel *et al.* [22] to calculate the width was inconsistent with that of Lane and Thomas [58].

In 1964, Armitage and Meads [24] used the ^{10}B$(d, d')^{10}$B reaction to populate this state, and found a similar width of $\Gamma_{\rm c.m.} = 110(10)$ keV by fitting deuteron spectra. Similarly Auwärter and Meyer [25] in 1975, performed a ^{9}Be$(p, \gamma)^{10}$B measurement found a similar width by fitting broadened γ-ray emission spectra from the $E_x = 7.56$ MeV state to the $E_x = 5.17$ MeV broad state, see Fig. 7 of Auwärter and Meyer [25]. From the fit of this γ-ray emission data, a $\Gamma_{\rm c.m.} = 100(10)$ keV was found.

Additionally, the present study was able to track the movement of the $\approx$ 3400 keV γ-ray emission, shown in Fig. 14. From this study, it was observed that the branchings from the $E_\alpha = 1.078$ and 1.168 MeV resonances through $\beta_{\rm R/DC\to1740}$ were entirely from the broad resonance, within statistical uncertainty. This finding indicates that many of the very large $B(E2)$ and $B(M2)$ values previously reported should be revised.

VI. R-MATRIX ANALYSIS

Using the R-matrix [58] data analysis framework, `AZURE2` [59, 60], theoretical fits were performed in order to more confidently determine the width of the broad $\approx$1.2 MeV resonance. The alternative R-matrix parameterization of Brune [61] was used so that observable widths could be used directly as R-matrix fit parameters. The narrow resonances in the ^{6}Li$(\alpha, \gamma)^{10}$B reaction were not included in the R-matrix analysis. The measurements of Sprenkel *et al.* [22] and Dearnaley *et al.* [23] used targets of a thickness large enough that target effects needed to be included in the calculations as given in Table IV. Additional details can be found in Ref. [62].

TABLE IV: R-Matrix Experimental Effects Parameters for the `AZURE2` code.

Segments	Integration Points	Active Density
Dearnaley *et al.* [23]	50	1.51×10^{18}
Sprenkel *et al.* [22]	50	2.51×10^{18}
Present Study	50	1.00×10^{18}

In Sprenkel *et al.* [22], a 50 keV thick target was reported, whereas Dearnaley *et al.* [23] used targets varying between 10-20 μg/cm^2. From SRIM stopping power calculations [53], the Sprenkel *et al.* [22] target would have been nearly 25 μg/cm^2 with $n \approx 2.51\times10^{18}$ and the Dearnaley *et al.* [23] target would have had $n \approx 1.51\times10^{18}$ assuming an average of 15 μg/cm^2 for the target thickness. Implementing these target integration effects, a small reduction of about $\approx$5 keV in Γ_α was observed.

A simultaneous R-matrix fit of the data surrounding the $\approx$1.2 MeV resonance was performed. The fit included the ^{6}Li$(\alpha, \alpha)^6$Li elastic scattering data of Dearnaley *et al.* [23], and the ^{6}Li$(\alpha, \gamma)^{10}$B data of Sprenkel *et al.* [22] as well as the current data. For the ^{6}Li$(\alpha, \alpha)^6$Li data of Dearnaley *et al.* [23], detailed uncertainties are not given. The only uncertainty information in the text states that "The accuracy of the experimental points is estimated at 3%, except at the lowest energies and near the minima of the anomalies where the increased magnitude of the background correction raises the error to about 5%." Therefore, to be conservative, the maximum uncertainty of 5% has been used. Using the Markov-Chain Monte-Carlo code `BRICK` [63], the statistical and common mode uncertainties of the fit parameters for the broad resonance were estimated to be $\Gamma_\gamma = 0.0589(46)$ eV (7.8%) and $\Gamma_\alpha = 124.7(25)$ keV (2.0%). Given the small statistical uncertainty for Γ_α, driven by the numerous scattering data, model uncertainties were also significant. In particular, those from the channel radius and background level contributions were investigated. Channel radii between 4.7 and 6.0 fm were investigated and found to produce variations of $\approx$4%. The fit was quite insensitive to background level contributions, producing variations of only $\approx$2%. In addition, no uncertainty in the energy calibration is given for the data of Dearnaley *et al.* [23], so a $\pm$20 keV uncertainty was assumed, which was found to produce a width variation of $\approx$4%. Different target thickness were also used by Dearnaley *et al.* [23], varying between 10 and 20 μg/cm^2. The present fit used an average value of 15 μg/cm^2, thus the $\pm5\mu$g/cm^2 target thickness uncertainty leads to an uncertainty of $\approx$1%. Given these additional contributions, the total uncertainty increases to 6.3%, giving $\Gamma_\alpha = 125(8)$ keV. The R-matrix fits for these data are shown in Figs. 4, 16, and 15.

Using the channel radius of 4.9 fm used by Dearnaley

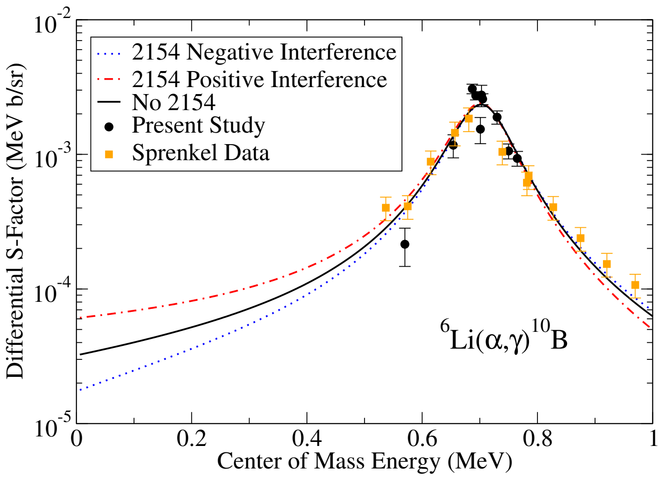

FIG. 15: Possible interference patterns with the subthreshold state at $E_x = 2154$ keV for the transition to the second excited state ($E_x = 1740$ keV) at $\theta = 45°$. The uncertainties in the current data are not able to distinguish between the two solutions. The upper limit DC component for the $E_x = 2154$ keV state is shown in green for comparison.

et al. [23], we find a reduced width of $\theta^2 = 1.82(11)$ MeV, in good agreement with the value of 1.8 MeV quoted in that work. While it should be noted that the Wigner limit is not a strict upper limit but only a limit on the average reduced width [64], Dearnaley *et al.* [23] have made the argument that this state corresponds to a cluster state of two α-particles and a deuteron. Thus the Wigner limit should be twice the usual value, owing to the two identical α-particles. As twice the Wigner limit would be $2 \times \gamma_{\mathrm{W}}^2 = 2{\times}0.929$ MeV $= 1.85$ MeV, this state would be a nearly pure cluster state of this type.

The R-matrix particle pair inputs are given in Table V, segments are given in Table VI, experimental effects are given in Table IV and fit parameters are given in Table VII. The normalization factor for the Dearnaley *et al.* [23] and Sprenkel *et al.* [22] were allowed to vary, since both sets were not given as absolute cross-sections in literature. In addition, error bars for these data were generated based on discussions found in these literature. The error bars for the Sprenkel *et al.* [22] data were assumed to be at minimum 10% and the Dearnaley *et al.* [23] data were assumed to be at minimum 5%.

VII. REACTION RATES

Sec. I described the potential role of the ^{6}Li$(\alpha,\gamma)^{10}$B reaction in first star nucleosynthesis. In the following, the contributions of the different reaction components to the reaction rate are described in more detail. Two calculations are the focus of this section, one with only the known resonance contributions, one that includes both non-resonant tails of subthreshold and higher energy states as well as direct capture contributions. Representative rate values for each component are quoted at $T = 0.1$ GK to help illustrate the effect of each to the total rate.

Previously, the rate of the ^{6}Li$(\alpha,\gamma)^{10}$B reaction commonly used in nucleosynthesis simulations is that of Thermonuclear Nuclear Reaction Rates V [26]. These tabulations are based on the estimate of an underlying direct capture component with individual known resonances being added separately. Specifically, two resonance contributions are considered [65]. The first is a single narrow resonance located at ≈500 keV with a resonance strength $\omega\gamma = 0.0462$ eV, as based on the measurements by Spear *et al.* [20]. This would correspond to the 3^+ state at 4.773 MeV in the compound nucleus ^{10}B. The second term refers to the sum of the tail distributions of higher energy resonances with a cut-off term at ≈1044 keV [65].

In the present analysis, three narrow and one broad resonance have been mapped. The DC component may exist, but has not been observed experimentally and spectroscopic factors remain unknown [17]. An upper limit for the DC contribution and its possible contribution to the overall reaction rate are considered below.

A. Resonance contributions

The narrow resonance contributions to the reaction rate were calculated individually using the narrow resonance approximation [66] and their individual contributions to the total rate are shown in Fig. 17. The $E_\alpha = 519.6(5)$ keV resonance is one of the main contributors to the rate, with a resonance strength of $\omega\gamma = 0.0472(37)$ eV; it's contribution dominates the reaction rate in the temperature range of $0.1 < T < 1$ GK. At 0.1 GK, its rate contribution is $1.13(6){\times}10^{-11}$ cm^3 mol^{-1} s^{-1}, where it competes with the low energy tail of the broad higher energy resonance at ≈1.2 MeV.

The two other observed narrow resonances are located at higher energies $E_\alpha = 1078.2(20)$ and $1168.3(20)$ keV. These resonance are fairly strong, with resonance strengths of $\omega\gamma = 0.0456(36)$ eV and $\omega\gamma = 0.389(30)$ eV, respectively. However, at 0.1 GK, due to their higher energy, they only have reaction rate contributions of $1.17(7){\times}10^{-28}$ and $2.27(12){\times}10^{-30}$ cm^3 mol^{-1} s^{-1}, respectively. At higher temperatures, above ≈2 GK, the $E_\alpha = 1078.2(20)$ keV resonance dominates the rate. The $E_\alpha = 1168.3(20)$ keV makes its largest contribution to the rate over a similar temperature range, but is always a weaker component.

The contribution from the broad resonance at $E_\alpha \approx 1.2$ MeV, which is found in this work to be at $E_\alpha = 1180$ keV, dominates the reaction rate in the low temperature range $T < 0.1$ GK. The value at 0.1 GK is $7.01{\times}10^{-11}$ cm^3 mol^{-1} s^{-1}.The resonance also makes a substantial contribution to the rate above ≈2 GK, becoming almost equal to that from the $E_\alpha = 1168$ keV resonance at 10 GK.

TABLE V: R-Matrix Particle Pair Parameters used for the `AZURE2` code.

Light Particle	Light Mass	Heavy Particle	Heavy Mass	E_x (MeV)	Separation Energy (MeV)	Channel Radius (fm)
α	4.0026	^{6}Li	6.01512	0	4.4611	5.5
γ_0	0	^{10}B	10.0129	0	0	0
γ_1	0	^{10}B	10.0129	0.71838	0	0
γ_2	0	^{10}B	10.0129	1.74005	0	0
γ_3	0	^{10}B	10.0129	2.15427	0	0
γ_4	0	^{10}B	10.0129	3.58713	0	0
p	1.00783	^{9}Be	9.01218	0	6.5867	5.5

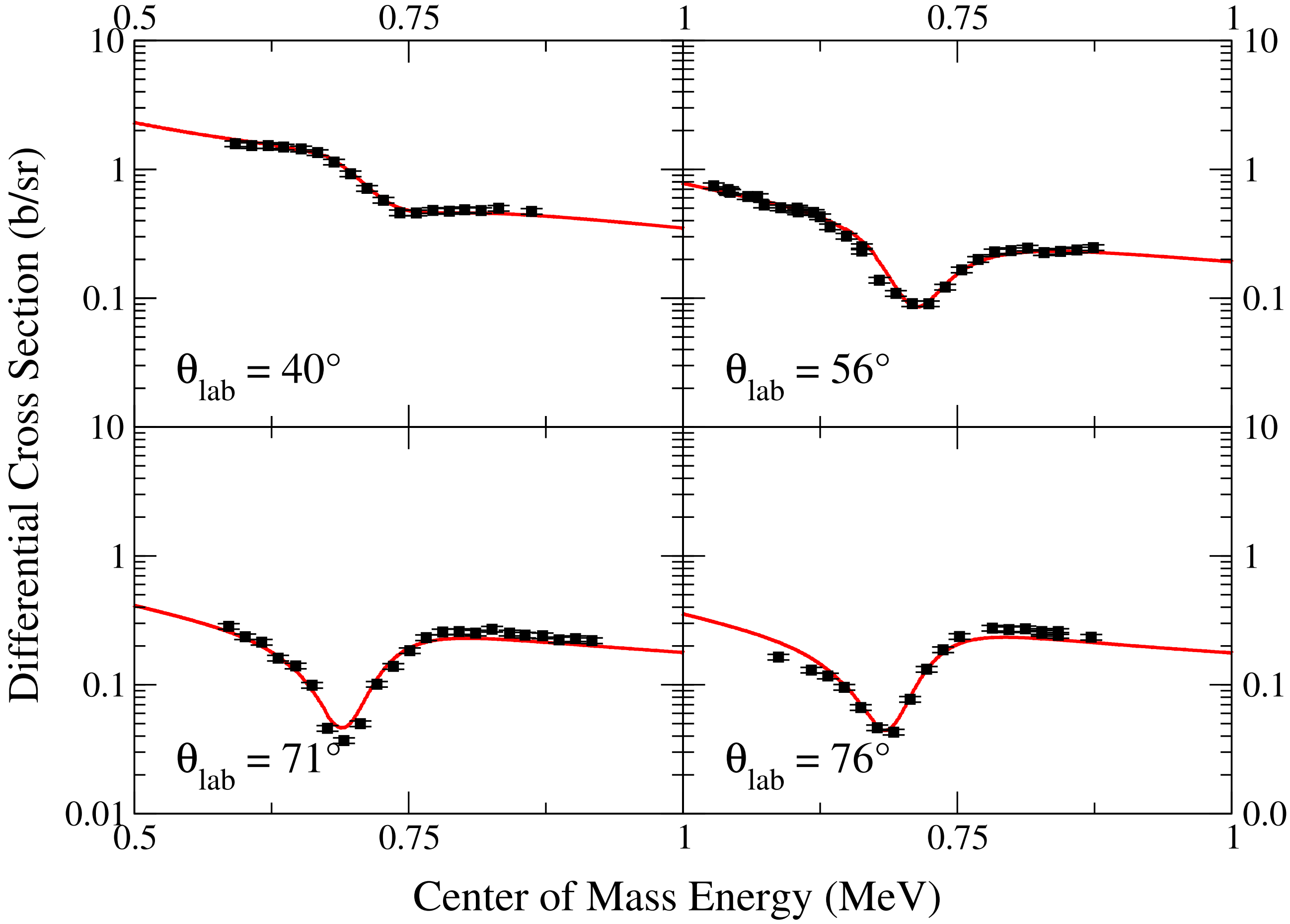

FIG. 16: R-Matrix fit of the ^{6}Li(α,α)^{6}Li elastic scattering data of Dearnaley *et al.* [23] at the lab angles of 40, 56, 71, and 76°.

TABLE VI: R-Matrix Segment Parameters.

Data set	Ref.
^{6}Li(α, α) @ 40° - 76°	Dearnaley *et al.* [23]
^{6}Li(α, γ)	Sprenkel *et al.* [22]

Compared to the present study, the reaction rate used by Caughlan and Fowler [26] is slightly smaller below 0.1 GK, by about 15%. This difference is entirely attributable to the difference in the tail contribution from the broad 1.2 MeV resonance. In Caughlan and Fowler [26], as with all the previous rate calculations for the ^{6}Li(α,γ)^{10}B reaction in that series, the larger width of 200 keV given by Sprenkel *et al.* [22] was used, and the smaller width of ≈100 keV found in the later works of Dearnaley *et al.* [23], Armitage and Meads [24] and Auwärter and Meyer [25] was not considered. It was therefore expected that this larger width should have pro-

TABLE VII: R-Matrix Fit Parameters.

E_x (MeV)	J^π	Partial Width	ℓ	s	Γ (eV)
6.8730	1^-				
		Γ_α	1	1	67000
		Γ_{γ_1}	1	1	0.24
		Γ_{γ_2}	1	0	0.64
		Γ_{γ_3}	1	1	0.16
		Γ_p	0	1	53000
5.1699	1^+				
		Γ_α	0	1	124700
		Γ_{γ_2}	1	0	0.058906
5.9220	2^+				
		Γ_α	2	1	5820
		Γ_{γ_0}	2	3	0.130
		Γ_{γ_1}	1	1	0.02
6.0240	4^+				
		Γ_α	4	1	52.0
		Γ_{γ_0}	1	3	0.11

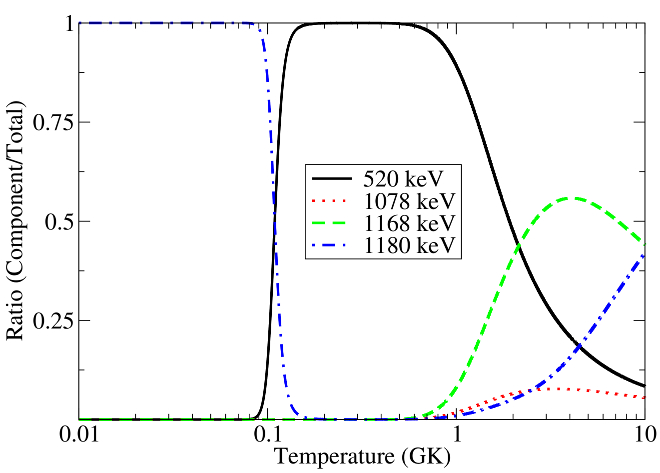

FIG. 17: Reaction rate contributions comparison for the ^{6}Li(α,γ)^{10}B reaction where only resonances with known strengths are included.

duced a larger reaction rate than the present calculation, but the opposite is true. Unfortunately, details on the calculation of the reaction rate given by Caughlan and Fowler [26] (and their previous works) is incomplete. Reconstructing the S-factor from the equation for the rate given by Caughlan and Fowler [26] does indeed produce a somewhat larger value, consistent with the reaction rate. The ratio of the rate as a function of temperature is illustrated in Fig. 18.

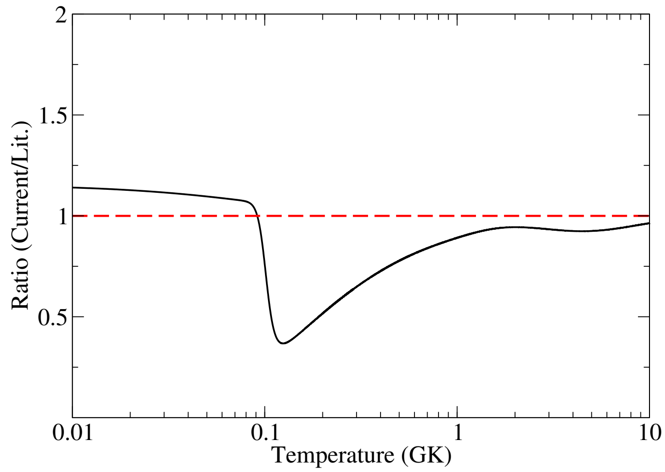

FIG. 18: Reaction rate ratio comparison to that of Caughlan and Fowler [26], taken from the Reaclib data base [14]. The position of the $E_\alpha = 520$ keV resonance has a significant impact on the reaction rate. Prior calculations put it at $E_\alpha = 500$ keV.

B. Inclusion of DC and subthreshold states

Because the DC components to the different bound states of ^{10}B may play a role at low temperatures, upper limits for these DC components were modeled using the external capture formalism [67–69] (EC) of the R-matrix code `AZURE2` and the direct capture (DC) potential model formalism of Rolfs [70] of the code `JEZEBEL` [28]. The DC S-factors were calculated for the transitions to the ground state (GS) up to the fourth excited state in ^{10}B as shown in Fig. 19. It was found that the GS transition is the dominant component and the energy dependence of the different models were similar. A hard-sphere (HS) EC calculation is used in `AZURE2`, whereas `JEZEBEL` uses a Wood-Saxon potential to calculate the DC contribution. The upper limit for the direct component, which would correspond to a pure alpha cluster configuration of ^{6}Li becomes comparable with the broad resonance contribution at $E_{\rm c.m.} \approx 0.17$ MeV, which corresponds to $E_\alpha \approx 0.28$ MeV, and a temperature of $\approx$0.18 GK.

In addition to the DC contributions to the reaction rate, possible interference between the broad 1.2 MeV resonance ($J^\pi = 1^+$) and a subthreshold state could enhance the low energy S-factor. Considering the subthreshold 1^+ levels, only the subthreshold state present at E_x =2154 keV ($E_{\rm c.m.}$ = -2307 keV) has a strong transition to the E_x = 1740 keV bound state similar to the 1.2 MeV unbound state [17]. It should be noted that DC to the second excited state is not possible from selection rules, as it is a 0^+ state. The subthreshold state contribution was calculated in `AZURE2` using the different interference possibilities between the broad resonance and the subthreshold resonance. The Γ_γ for the state was taken from the TUNL database [17] and the branching ratios from the present study were used. The ANC for

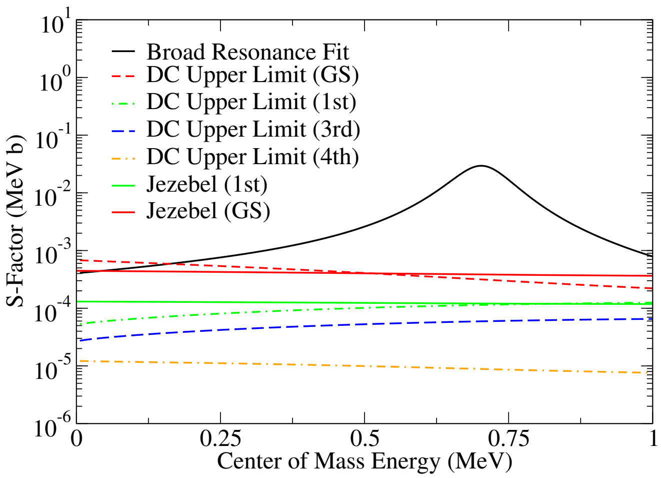

FIG. 19: Comparison of the S-factor of various direct reaction components. The upper limit for direct component to several of the bound states in ^{10}B is shown. The strongest contributions come from the GS transition, as shown in red (solid line for `JEZEBEL`, dashed for `AZURE2`).

the subthreshold state was set at the Wigner limit of the corresponding reduced width amplitude, 72 fm$^{-1/2}$. Using these upper limit values, it was found that significant interference with the tailing of the broad ≈1.2 MeV resonance at low energy is possible, as shown in Fig. 15. This interference occurs below the presently explored energy range, making this a significant source of uncertainty at temperatures below 0.1 GK. An extension of the measurements towards lower energies would require improved cosmic ray shielding as given at underground accelerators [71, 72].

By including the subthreshold state and DC components, a maximal reaction rate can be calculated. The DC components that have the highest impact are the transitions to the ground state and the first excited state. The subthreshold effects of the third excited state in ^{10}B could also be significant through its interference with the broad resonance at $E_\alpha \approx 1.2$ MeV. The impact of these additional components can be seen in the upper limit reaction rate calculation presented in Fig. 20. The individual contributions to the upper limit reaction rate are given in Fig. 21. An upper limit of 1.2×10^{-10} cm^3 mol^{-1} s^{-1} was found at $T = 0.1$ GK for comparison.

C. Recommended Rates

From the above calculations, the central, upper, and lower bounds of the reaction rate have been calculated as follows:

- Central value — The central value has been calculated using the central values of the resonance strengths and energies given in Table III. The contribution from the broad 1.2 MeV resonance is included by numerical integration of the R-matrix fit described in Sec. VI, without any subthreshold state interference. No direct capture contribution is included.

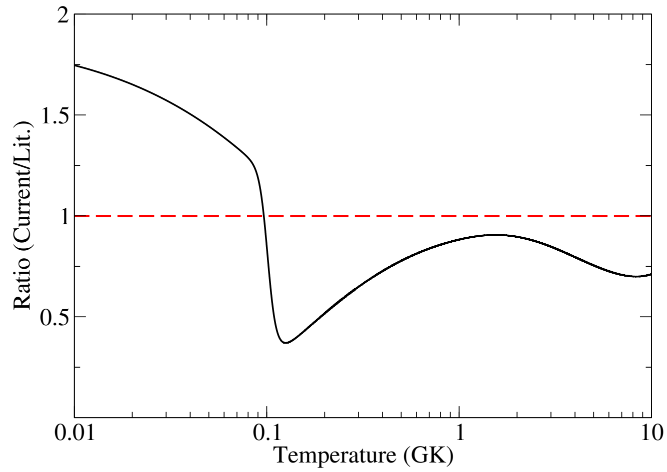

FIG. 20: Reaction rate ratio comparing the present rate with the one given by Caughlan and Fowler [26] as in Fig. 18, but the upper limit DC and subthreshold $E_x = 2154$ keV state contributions are included.

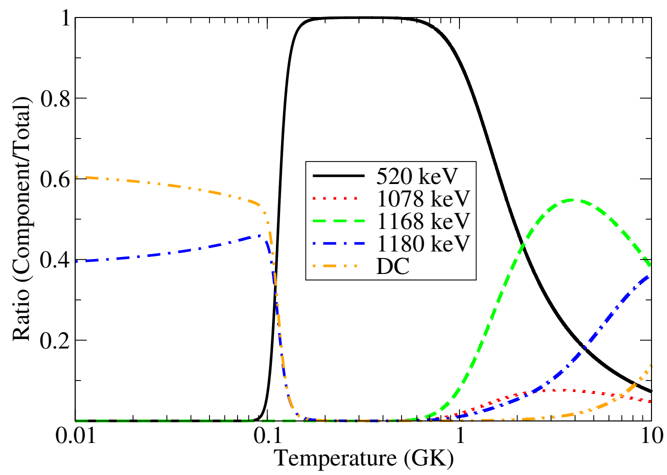

FIG. 21: Reaction rate contributions comparison using the upper limit for the DC and interference with the subthreshold state described in the text. Below 0.1 GK, the GS DC and broad $E_\alpha \approx 1.2$ MeV resonance with subthreshold state interference in the third excited state transition dominate the rate.

- Upper limit — The upper limit has been calculated using the lower values of the resonance energies and the upper values of the resonance strengths given in Table III. The increased low energy S-factor interference solution from the R-matrix calculation (see Fig. 15), that includes the 1.2 MeV resonance and the subthreshold state, has been used as described

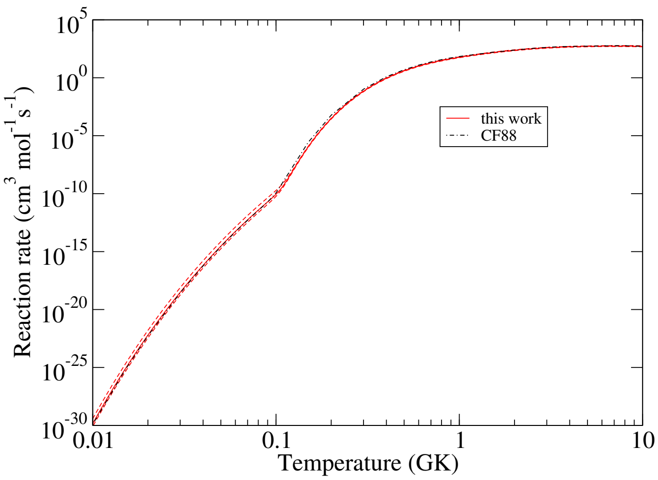

FIG. 22: The ^{6}Li(α,γ)^{10}B reaction rate based on the measurements of this work. The rate of Caughlan and Fowler [26] (CF88) is also shown for comparison.

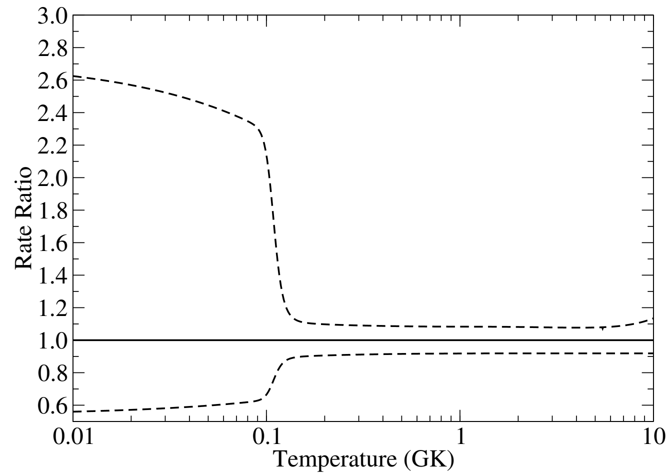

FIG. 23: Ratio of the upper and lower limits of the ^{6}Li(α,γ)^{10}B reaction rate to its recommended median value.

in Sec. VII B. Upper limits for the direct capture contributions are also included.

- Lower limit — The lower limit has been calculated using the upper values for the energies and lower values for the resonance strengths given in Table III. The decreased low energy S-factor interference solution from the R-matrix calculation (see Fig. 15), that includes the 1.2 MeV resonance and the subthreshold state, has been used as described in Sec. VII B. No direct capture contribution is included.

While the reaction rate uncertainties above 0.1 GK can be treated as 1σ uncertainties of a Gaussian distributed underlying probability density function (PDF) for the reaction rate, the uncertainties at lower temperatures should be treated as classical upper and lower limits. This is because the uncertainties below 0.1 GK come from the uncertainty in the interference of the tail contribution of the 1.2 MeV, broad resonance, which has been calculated by assuming full clusterization (the maximum value) for the reduced widths of the bound states used to calculate the subthreshold and DC contributions. The reaction rate is given in Table VIII, while a rate tabulated on a finer temperature grid is available in the Supplemental Material [73]. The reaction rate is shown in Fig. 22, compared with that of Caughlan and Fowler [26], and the relative rate uncertainty is shown in Fig. 23.

VIII. CONCLUSION

New measurements of the low energy excitation function for the ^{6}Li(α,γ)^{10}B reaction at $\theta_{Lab} = 55°$ are presented with angular distributions for the $E_\alpha = 1078$ and 1168 keV resonances. The new data have been used to provide both improved data on the narrow resonance strengths and to better characterize the broad resonance, DC, and direct components that influence the low energy S-factor. New strengths for the three narrow resonance at $E_\alpha = 519.6(5)$, 1078.2(20) and 1168.3(20) keV are derived from the present measurements.

The two identical α-particle cluster structure of the state at 5.17 MeV has been confirmed by performing a multichannel R-matrix analysis that includes ^{6}Li(α,γ_2)^{10}B data from the present work, that of Sprenkel *et al.* [22] and the ^{6}Li(α,α)^{6}Li scattering data of Dearnaley *et al.* [23]. The interpretation of this unique nuclear structure is a prime candidate for theoretical investigations using ab-initio theory. Further, an investigation was made of the possible inteference of the tail of this broad resonance with the subthreshold state in ^{10}B at $E_x = 2.154$ MeV, showing that a significant effect on the low energy cross section is possible, if the subthreshold state has a α-cluster structure. This also motivates both future ab-initio calculations and α-transfer measurements to better characterize the α-cluster structure of this bound state in ^{10}B.

Using these results, new upper and lower limits for the reaction rate have been calculated. At temperatures below 0.1 GK, the present study finds a lower limit that is larger than the recommended value of Caughlan and Fowler [26]. This is due to their use of a lower energy for the $E_\alpha = 519.6(5)$ keV resonance of $E_\alpha = 500(25)$ keV. The high likelihood of subthreshold cluster states results in a larger upper limit than that estimated previously. This is the result of the inclusion of broad resonance interference, DC, and subthreshold state contributions. This results in a minimum increase in the reaction rate of ≈15% and a maximum increase of ≈85% compared to that of CF88 [26]. An additional increase of the reaction rate can be suggested based on the d-α structure of ^{6}Li, which has been suggested to lead to an effective reduction in electron screening in a high density plasma environment as suggested by Spitaleri *et al.* [74]. This effect is reflected by the screening potential in low energy laboratory experiments being systematically higher than the values predicted for spherical nuclei [75]. To verify this effect in a laboratory environment for the ^{6}Li$(\alpha,\gamma)^{10}$B reaction would require following the cross section measurements towards lower energies. The impact on the stellar reaction rate would depend on the highly dynamic density conditions in the first star environment and can only be evaluated in that context.

The impact of the here suggested enhanced reaction rate in early star nucleosynthesis also depends sensitively on the seed abundance for ^{4}He and the equilibrium abundance of ^{6}Li that is expected to be reached as a consequence of the associated production and depletion reactions in the early star environment [76]. The latter depends also on the depletion rate of the compound nucleus ^{10}B via subsequent proton [77] and alpha induced reaction mechanisms [78]. These reactions are being addressed independently. The nucleosynthesis conditions are not only characterized by a complex dynamic reaction network driven by these reactions, but also depend sensitively on dynamic mixing and the emergence of helium rich hydrogen poor bubbles [12]. This discussion is beyond the scope of this paper and will be addressed in a forthcoming study.

ACKNOWLEDGMENTS

This research utilized resources from the Notre Dame Center for Research Computing and was supported by the National Science Foundation through Grant No. PHY-1713857 and PHY-2011890, and the Joint Institute for Nuclear Astrophysics through Grant No. PHY-1430152 (JINA Center for the Evolution of the Elements).

[1] R. H. Cyburt, B. D. Fields, K. A. Olive, and T.-H. Yeh, Big Bang nucleosynthesis: Present status, Rev. Mod. Phys. **88**, 015004 (2016).

[2] V. Bromm and R. B. Larson, The First Stars, Annual Review of Astronomy and Astrophysics **42**, 79 (2004).

[3] E. G. Adelberger, A. García, R. G. H. Robertson, K. A. Snover, A. B. Balantekin, K. Heeger, M. J. Ramsey-Musolf, D. Bemmerer, A. Junghans, C. A. Bertulani, J.-W. Chen, H. Costantini, P. Prati, M. Couder, E. Uberseder, M. Wiescher, R. Cyburt, B. Davids, S. J. Freedman, M. Gai, D. Gazit, L. Gialanella, G. Imbriani, U. Greife, M. Hass, W. C. Haxton, T. Itahashi, K. Kubodera, K. Langanke, D. Leitner, M. Leitner, P. Vetter, L. Winslow, L. E. Marcucci, T. Motobayashi, A. Mukhamedzhanov, R. E. Tribble, K. M. Nollett, F. M. Nunes, T.-S. Park, P. D. Parker, R. Schiavilla, E. C. Simpson, C. Spitaleri, F. Strieder, H.-P. Trautvetter, K. Suemmerer, and S. Typel, Solar fusion cross sections. II. The *pp* chain and CNO cycles, Rev. Mod. Phys. **83**, 195 (2011).

[4] M. Wiescher, J. Görres, S. Graff, L. Buchmann, and F. K. Thielemann, The Hot Proton-Proton Chains in Low-Metallicity Objects, ApJ **343**, 352 (1989).

[5] A. Heger and S. E. Woosley, Nucleosynthesis and evolution of massive metal-free stars, The Astrophysical Journal **724**, 341 (2010).

[6] M. Wiescher, R. deBoer, J. Görres, A. Gula, and Q. Liu, Neutron sources in early stars, Acta Phys. Pol. B **51**, 631 (2020).

[7] A. J. Elwyn, R. E. Holland, C. N. Davids, L. Meyer-Schützmeister, F. P. Mooring, and W. Ray, Cross sections for the ^{6}Li$(p,^{3}$He$)^{4}$He reaction at energies between 0.1 and 3.0 MeV, Phys. Rev. C **20**, 1984 (1979).

[8] J. Cruz, H. Luis, M. Fonseca, Z. Fülöp, G. Gyürky, F. Raiola, M. Aliotta, K. U. Kettner, A. P. Jesus, J. P. Ribeiro, F. C. Barker, and C. Rolfs, Experimental study of proton-induced nuclear reactions in ^{6,7}Li, Journal of Physics G: Nuclear and Particle Physics **35**, 014004 (2007).

[9] M. Wiescher, R. J. deBoer, J. Görres, and R. E. Azuma, Low energy measurements of the ^{10}B$(p,\alpha)^{7}$Be reaction, Phys. Rev. C **95**, 044617 (2017).

[10] K. Ikeda, T. Marumori, R. Tamagaki, and H. Tanaka, Chapter I. Formation of the Viewpoint, Alpha-Like Four-Body Correlations and Molecular Aspects in Nuclei, Prog. Theor. Phys. Suppl. **52**, 1 (1972), http://oup.prod.sis.lan/ptps/article-pdf/doi/10.1143/PTPS.52.1/5357826/52-1.pdf.

[11] G. Gyürky, Z. Fülöp, E. Somorjai, G. Kiss, and C. Rolfs, Absolute resonance strengths in the ^{6,7}Li$(\alpha,\gamma)^{10,11}$B reactions, The European Physical Journal A - Hadrons and Nuclei **21**, 355 (2004).

[12] O. Clarkson and F. Herwig, Convective H-He interactions in massive population III stellar evolution models, Monthly Notices of the Royal Astronomical Society **500**, 2685 (2020), https://academic.oup.com/mnras/article-pdf/500/2/2685/34546031/staa3328.pdf.

[13] D. H. Wilkinson and G. A. Jones, The Reaction Li$^{6}(\alpha,\gamma)$B^{10}, Phys. Rev. **91**, 1575 (1953).

[14] R. H. Cyburt, A. M. Amthor, R. Ferguson, Z. Meisel, K. Smith, S. Warren, A. Heger, R. D. Hoffman, T. Rauscher, A. Sakharuk, H. Schatz, F. K. Thielemann, and M. Wiescher, The JINA REACLIB Database: Its Recent Updates and Impact on Type-I X-Ray Bursts, The Astrophysical Journal Supplement Series **189**, 240 (2010).

[15] J. E. Nelson, J. Napolitano, and S. J. Freedman, E2 strength of the lowest resonance in ^{6}Li(α,γ): Collective effects in the 1p shell, Phys. Rev. C **31**, 2295 (1985).

[16] D. E. Alburger, P. D. Parker, D. J. Bredin, D. H. Wilkinson, P. F. Donovan, A. Gallmann, R. E. Pixley, L. F. Chase, and R. E. McDonald, Properties of the 4.77- and 5.16-MeV States of B^{10}, Phys. Rev. **143**, 692 (1966).

[17] D. Tilley, J. Kelley, J. Godwin, D. Millener, J. Purcell, C. Sheu, and H. Weller, Energy levels of light nuclei A = 8,9,10, Nuclear Physics A **745**, 155 (2004).

[18] J. Napolitano and S. Freedman, The width of the 5.11 MeV state in ^{10}B and isovector parity mixing, Nuclear

Physics A **417**, 289 (1984).

[19] P. Forsyth, H. Tu, and W. Hornyak, The ^{6}Li(α, γ)^{10}B reaction and the energy levels of ^{10}B, Nuclear Physics **82**, 33 (1966).

[20] R. Spear, Z. Switkowski, D. Kennedy, and J. Heggie, Resonance strength of the 1175 keV resonance in ^{6}Li(α, γ)^{10}B, Nuclear Physics A **318**, 21 (1979).

[21] R. E. Segel, P. P. Singh, S. S. Hanna, and M. A. Grace, Gamma Rays from $B^{10} + p$; Decay Schemes and Excitation Functions, Phys. Rev. **145**, 736 (1966).

[22] E. L. Sprenkel, J. W. Olness, and R. E. Segel, Identification of Doublet States at 5.16 MeV in B^{10}, Phys. Rev. Lett. **7**, 174 (1961).

[23] G. Dearnaley, D. Gemmell, and S. Hanna, States in B^{10} from elastic scattering of alphas by Li^{6}, Nuclear Physics **36**, 71 (1962).

[24] B. Armitage and R. Meads, Levels in B^{10} above 5.16 MeV observed by proton and deuteron inelastic scattering, Physics Letters **8**, 346 (1964).

[25] W. Auwärter and V. Meyer, Excited states of ^{10}B from the ^{6}Li(α, γ) and ^{9}Be(p, γ) reactions, Nuclear Physics A **242**, 129 (1975).

[26] G. R. Caughlan and W. A. Fowler, Thermonuclear reaction rates V, Atomic Data and Nuclear Data Tables **40**, 283 (1988).

[27] Y. Kanada-En'yo, T. Suhara, and Y. Taniguchi, Approximation of reduced width amplitude and application to cluster decay width, Progress of Theoretical and Experimental Physics **2014**, 10.1093/ptep/ptu095 (2014), 073D02, https://academic.oup.com/ptep/article-pdf/2014/7/073D02/19300894/ptu095.pdf.

[28] M. Wiescher, H. Becker, J. Görres, K.-U. Kettner, H. Trautvetter, W. Kieser, C. Rolfs, R. Azuma, K. Jackson, and J. Hammer, Nuclear and astrophysical aspects of ^{18}O$(p, \gamma)^{19}$F, Nuclear Physics A **349**, 165 (1980).

[29] H. Nishioka, Two-alpha-particle-plus-dinucleon-cluster model for ^{10}B and ^{10}Be, Journal of Physics G: Nuclear Physics **10**, 1713 (1984).

[30] A. V. Nesterov, V. S. Vasilevsky, and T. P. Kovalenko, Spectrum of Bound States of Nucleus ^{10}B in a Three-Cluster Microscopic Model, Ukrainian Journal of Physics **59**, 1065 (2018).

[31] ISNAP Accelerators (2021).

[32] A. Antilla, J. Keinonen, M. Hautala, and I. Forsblom, Use of the ^{27}Al$(p, \gamma)^{28}$Si, $E_p = 992$ keV resonance as a gamma-ray intensity standard, Nuclear Instruments and Methods **147**, 501 (1977).

[33] G. Hardie, B. W. Filippone, A. J. Elwyn, M. Wiescher, and R. E. Segel, Resonant alpha capture by ^{7}Be and ^{7}Li, Phys. Rev. C **29**, 1199 (1984).

[34] G. Gilardy, *Measuring the* $^{7}Li(\alpha, \gamma)^{11}B$ *reaction rate at temperatures relevant for the n-process*, Theses, Université de Bordeaux (2018).

[35] S. Croft, The absolute yield, angular distribution and resonance widths of the 6.13, 6.92 and 7.12 MeV photons from the 340.5 keV resonance of the ^{19}F$(p, \alpha\gamma)^{16}$O reaction, Nuclear Instruments and Methods in Physics Research Section A: Accelerators, Spectrometers, Detectors and Associated Equipment **307**, 353 (1991).

[36] C. Angulo, M. Arnould, M. Rayet, P. Descouvemont, D. Baye, C. Leclercq-Willain, A. Coc, S. Barhoumi, P. Aguer, C. Rolfs, R. Kunz, J. Hammer, A. Mayer, T. Paradellis, S. Kossionides, C. Chronidou, K. Spyrou, S. Degl'Innocenti, G. Fiorentini, B. Ricci, S. Zavatarelli, C. Providencia, H. Wolters, J. Soares, C. Grama, J. Rahighi, A. Shotter, and M. L. Rachti, A compilation of charged-particle induced thermonuclear reaction rates, Nucl. Phys. A **656**, 3 (1999).

[37] R. J. deBoer, O. Clarkson, A. J. Couture, J. Görres, F. Herwig, I. Lombardo, P. Scholz, and M. Wiescher, ^{19}F$(p, \gamma)^{20}$Ne and ^{19}F$(p, \alpha)^{16}$O reaction rates and their effect on calcium production in Population III stars from hot CNO breakout, Phys. Rev. C **103**, 055815 (2021).

[38] J. McQuaid, The Performance of CeBr3 Detectors (2019).

[39] E. Browne and J. Tuli, Nuclear Data Sheets for $A = 137$, Nuclear Data Sheets **108**, 2173 (2007).

[40] Y. Khazov, A. Rodionov, and F. Kondev, Nuclear Data Sheets for $A = 133$, Nuclear Data Sheets **112**, 855 (2011).

[41] eckert and ziegler reference and calibration source (2007).

[42] E. Browne and J. Tuli, Nuclear Data Sheets for $A = 60$, Nuclear Data Sheets **114**, 1849 (2013).

[43] H. Junde, H. Su, and Y. Dong, Nuclear Data Sheets for $A = 56$, Nuclear Data Sheets **112**, 1513 (2011).

[44] W. D. Kulp, J. L. Wood, J. M. Allmond, J. Eimer, D. Furse, K. S. Krane, J. Loats, P. Schmelzenbach, C. J. Stapels, R.-M. Larimer, E. B. Norman, and A. Piechaczek, $n = 90$ region: The decays of ^{152}Eu^{m,g} to ^{152}Sm, Phys. Rev. C **76**, 034319 (2007).

[45] M. Shamsuzzoha Basunia, Nuclear Data Sheets for $A = 210$, Nuclear Data Sheets **121**, 561 (2014).

[46] Standard Electrode Coaxial Ge Detectors (2020).

[47] A. Basak, Parity-violating effects in the ^{6}Li$(\alpha, \gamma)^{10}$B capture reaction via the 5.1 MeV doublet resonance, Nuclear Physics A **499**, 353 (1989).

[48] C. Illiadis, *Nuclear Physics of Stars* (Wiley-VCH, Weinheim, Germany, 2015).

[49] G. J. McCallum and G. E. Coote, Influence of source-detector distance on relative intensity and angular correlation measurements with Ge(Li) spectrometers, Nuclear Instruments and Methods **130**, 189 (1975).

[50] E. T. Yoon, M. Y. Kang, I. J. Kim, G. M. Sun, and H.-D. Choi, Coincidence summing correction for a voluminous ^{152}Eu source, Nuclear Engineering and Technology **52**, 1266 (2020).

[51] H. Warhanek, The 4.77 MeV Level in Boron 10, The Philosophical Magazine: A Journal of Theoretical Experimental and Applied Physics **2**, 1085 (1957), https://doi.org/10.1080/14786435708242736.

[52] L. Meyer-Schutzmeister and S. S. Hanna, Energy Levels in B^{10} in the Reaction $Li^{6}(\alpha,\gamma)B^{10}$, Physical Review **108**, 1506 (1957).

[53] J. Ziegler, Srim - the stopping and range of ions in matter (2010).

[54] F. Ajzenberg and T. Lauritsen, Energy Levels of Light Nuclei. IV, Rev. Mod. Phys. **24**, 321 (1952).

[55] F. Ajzenberg-Selove, Energy levels of light nuclei $A = 5$–10, Nuclear Physics A **320**, 1 (1979).

[56] P. Bizzeti and A. Perego, The ^{4}He(^{6}Li,γ)^{10}B reaction as a possible test on weak-interaction models, Physics Letters B **64**, 298 (1976).

[57] F. Ajzenberg-Selove, Energy levels of light nuclei A = 5-10, Nuclear Physics A **490**, 1 (1988).

[58] A. M. Lane and R. G. Thomas, R-matrix theory of nuclear reactions, Rev. Mod. Phys. **30**, 257 (1958).

[59] R. E. Azuma, E. Uberseder, E. C. Simpson, C. R. Brune, H. Costantini, R. J. de Boer, J. Görres, M. Heil, P. J. LeBlanc, C. Ugalde, and M. Wiescher, AZURE: An *R*-

matrix code for nuclear astrophysics, Phys. Rev. C **81**, 045805 (2010).

[60] E. Uberseder and R. J. deBoer, *AZURE2 User Manual* (2015).

[61] C. R. Brune, Alternative parametrization of R -matrix theory, Phys. Rev. C **66**, 044611 (2002).

[62] A. Gula, *An Alternative 3α Process: The $^2H(\alpha,\gamma)^6Li(\alpha,\gamma)^{10}B(\alpha,d)^{12}C$ Reaction in Primordial Stars*, Ph.D. thesis, Dept. of Physics, University of Notre Dame, Notre Dame, IN, USA (2022).

[63] D. Odell, C. Brune, D. Phillips, R. deBoer, and S. Paneru, Performing Bayesian analyses with AZURE2 using BRICK: an application to the ^{7}Be system (2022), unpublished.

[64] C. B. Dover, C. Mahaux, and H. A. Weidenmüller, The single-particle limit for partial widths, Nuclear Physics A **139**, 593 (1969).

[65] M. Harris, Notes to "Thermonuclear Reaction rates III", Orange Aid Preprint (1982), Caltech, unpublished.

[66] W. A. Fowler, G. R. Caughlan, and B. A. Zimmerman, Thermonuclear Reaction Rates, II, Annual Review of Astronomy and Astrophysics **13**, 69 (1975), https://doi.org/10.1146/annurev.aa.13.090175.000441.

[67] R. J. Holt, H. E. Jackson, R. M. Laszewski, J. E. Monahan, and J. R. Specht, Effects of channel and potential radiative transitions in the ^{17}O$(\gamma, n_0)^{16}$O reaction, Phys. Rev. C **18**, 1962 (1978).

[68] F. C. Barker and T. Kajino, The ^{12}C$(\alpha,\gamma)^{16}$O Cross Section at Low Energies., Aust. J. Phys. **44**, 369 (1991).

[69] C. Angulo and P. Descouvemont, The ^{14}N$(p,\gamma)^{15}$O low-energy S-factor, Nucl. Phys. A **690**, 755 (2001).

[70] C. Rolfs, Spectroscopic factors from radiative capture reactions, Nuclear Physics A **217**, 29 (1973).

[71] D. Robertson, M. Couder, U. Greife, F. Strieder, and M. Wiescher, Underground nuclear astrophysics studies with CASPAR, Eur. J. Phys. Web of Conferences **109**, 09002 (2016).

[72] H. Costantini, A. Formicola, G. Imbriani, M. Junker, C. Rolfs, and F. Strieder, LUNA: a laboratory for underground nuclear astrophysics, Rep. Prog. Phys. **72**, 086301 (2009).

[73] See Supplemental Material at [URL will be inserted by publisher] for the reaction rate tabulated on a finer temperature grid.

[74] C. Spitaleri, C. Bertulani, L. Fortunato, and A. Vitturi, The electron screening puzzle and nuclear clustering, Physics Letters B **755**, 275 (2016).

[75] H. J. Assenbaum, K. Langanke, and C. Rolfs, Effects of electron screening on low-energy fusion cross sections, Zeitschrift für Physik A Atomic Nuclei **327**, 461 (1987).

[76] M. Wiescher, O. Clarkson, R. J. deBoer, and P. Denisenkov, Nuclear clusters as the first stepping stones for the chemical evolution of the universe., The European Physical Journal A **57**, 10.1140/epja/s10050-020-00339-x (2021).

[77] B. V. Kolk, K. T. Macon, R. J. deBoer, T. Anderson, A. Boeltzig, K. Brandenburg, C. R. Brune, Y. Chen, A. M. Clark, T. Danley, B. Frentz, R. Giri, J. Görres, M. Hall, S. L. Henderson, E. Holmbeck, K. B. Howard, D. Jacobs, J. Lai, Q. Liu, J. Long, K. Manukyan, T. Massey, M. Moran, L. Morales, D. Odell, P. O'Malley, S. N. Paneru, A. Richard, D. Schneider, M. Skulski, N. Sensharma, C. Seymour, G. Seymour, D. Soltesz, S. Strauss, A. Voinov, L. Wüstrich, and M. Wiescher, Investigation of the ^{10}B$(p,\alpha)^7$Be reaction from 0.8 to 2.0 MeV, Phys. Rev. C **105**, 055802 (2022).

[78] A. Gula, R. deBoer, K. Manukyan, M. Wiescher, R. Kelmar, S. Aguilar, S. Henderson, S. Moylan, B. F. J. Wilkinson, S. McGuinness, C. Seymour, S. Shahina, C. B. J. Arroyo, and J. Görres, Charge Particle ^{10}B+α Reactions at Low Energies (2022), unpublished.

TABLE VIII: Rate for the ^{6}Li$(\alpha,\gamma)^{10}$B reaction. A rate table on a finer temperature grid is available in the Supplemental Material [73].

T (GK)	Median	Minimum	Maximum
1.00×10^{-3}	1.19×10^{-73}	6.51×10^{-74}	3.22×10^{-73}
1.25×10^{-3}	7.89×10^{-68}	4.31×10^{-68}	2.13×10^{-67}
1.58×10^{-3}	2.67×10^{-62}	1.46×10^{-62}	7.18×10^{-62}
1.98×10^{-3}	3.48×10^{-57}	1.91×10^{-57}	9.37×10^{-57}
2.50×10^{-3}	1.89×10^{-52}	1.03×10^{-52}	5.06×10^{-52}
3.14×10^{-3}	4.51×10^{-48}	2.48×10^{-48}	1.21×10^{-47}
3.96×10^{-3}	5.08×10^{-44}	2.80×10^{-44}	1.35×10^{-43}
4.98×10^{-3}	2.84×10^{-40}	1.57×10^{-40}	7.55×10^{-40}
6.27×10^{-3}	8.29×10^{-37}	4.60×10^{-37}	2.20×10^{-36}
7.90×10^{-3}	1.33×10^{-33}	7.42×10^{-34}	3.51×10^{-33}
9.94×10^{-3}	1.23×10^{-30}	6.87×10^{-31}	3.22×10^{-30}
1.25×10^{-2}	6.76×10^{-28}	3.81×10^{-28}	1.77×10^{-27}
1.58×10^{-2}	2.32×10^{-25}	1.31×10^{-25}	6.01×10^{-25}
1.98×10^{-2}	5.12×10^{-23}	2.92×10^{-23}	1.32×10^{-22}
2.50×10^{-2}	7.52×10^{-21}	4.34×10^{-21}	1.92×10^{-20}
3.14×10^{-2}	7.59×10^{-19}	4.42×10^{-19}	1.91×10^{-18}
3.96×10^{-2}	5.41×10^{-17}	3.19×10^{-17}	1.34×10^{-16}
4.98×10^{-2}	2.80×10^{-15}	1.67×10^{-15}	6.85×10^{-15}
6.27×10^{-2}	1.08×10^{-13}	6.54×10^{-14}	2.59×10^{-13}
7.90×10^{-2}	3.16×10^{-12}	1.95×10^{-12}	7.42×10^{-12}
9.94×10^{-2}	8.15×10^{-11}	5.39×10^{-11}	1.76×10^{-10}
1.25×10^{-1}	1.34×10^{-8}	1.17×10^{-8}	1.67×10^{-8}
1.58×10^{-1}	3.30×10^{-6}	2.97×10^{-6}	3.74×10^{-6}
1.98×10^{-1}	2.62×10^{-4}	2.38×10^{-4}	2.93×10^{-4}
2.50×10^{-1}	7.92×10^{-3}	7.20×10^{-3}	8.78×10^{-3}
3.14×10^{-1}	1.11×10^{-1}	1.01×10^{-1}	1.22×10^{-1}
3.96×10^{-1}	8.36×10^{-1}	7.64×10^{-1}	9.17×10^{-1}
4.98×10^{-1}	3.89×10^{0}	3.56×10^{0}	4.25×10^{0}
6.27×10^{-1}	1.24×10^{1}	1.13×10^{1}	1.35×10^{1}
7.90×10^{-1}	2.95×10^{1}	2.71×10^{1}	3.21×10^{1}
9.94×10^{-1}	5.77×10^{1}	5.30×10^{1}	6.28×10^{1}
1.25×10^{0}	9.99×10^{1}	9.18×10^{1}	1.09×10^{2}
1.58×10^{0}	1.59×10^{2}	1.46×10^{2}	1.73×10^{2}
1.98×10^{0}	2.35×10^{2}	2.16×10^{2}	2.56×10^{2}
2.50×10^{0}	3.21×10^{2}	2.95×10^{2}	3.47×10^{2}
3.14×10^{0}	4.02×10^{2}	3.70×10^{2}	4.35×10^{2}
3.96×10^{0}	4.69×10^{2}	4.31×10^{2}	5.07×10^{2}
4.98×10^{0}	5.15×10^{2}	4.73×10^{2}	5.56×10^{2}
6.27×10^{0}	5.37×10^{2}	4.94×10^{2}	5.83×10^{2}
7.90×10^{0}	5.36×10^{2}	4.93×10^{2}	5.90×10^{2}
9.94×10^{0}	5.14×10^{2}	4.72×10^{2}	5.83×10^{2}